Endothelial cell signature in muscle stem cells showed by VEGFA-FLT1-AKT1 axis for muscle stem cell survival

Authors/Affiliations

Mayank Verma[a,b,c,d], Yoko Asakura[b,c,d], Xuerui Wang[b,c,d], Kasey Zhou[b,c,d], Mahmut Ünverdi[b,c,d], Allison P. Kann[e,f], Robert S. Kraus[e,f] and Atsushi Asakura[b,c,d]

Department of Pediatrics & Neurology, Division of Pediatric Neurology, The University of Texas Southwestern Medical Center, TX, USA[a].

Stem Cell Institute[b], Paul & Sheila Wellstone Muscular Dystrophy Center[c], Department of Neurology[d], University of Minnesota Medical School, MN, USA

Department of Cell, Developmental, and Regenerative Biology[e], and Graduate School of Biomedical Sciences[f], Icahn School of Medicine at Mount Sinai, NY, USA.

Conflict of Interest

MV and AA are listed as inventors on a patent for anti-FLT1 antibody mediated therapy for DMD. AA received consulting fees from ShireHGT.

Abstract

Endothelial and skeletal muscle lineages arise from common embryonic progenitors. Despite their shared developmental origin, adult endothelial cells (ECs) and muscle stem cells (MuSCs) (satellite cells) have been thought to possess distinct gene signatures and signaling pathways. Here we shift this paradigm by uncovering how adult MuSC behavior is affected by the expression of a subset of EC transcripts. We used several computational analyses including single-cell RNAseq to show that MuSCs express low levels of canonical EC markers. We demonstrate that MuSC survival is regulated by one such prototypic endothelial signaling pathway (VEGFA-FLT1). Using pharmacological and genetic gain- and loss-of-function studies, we identify the FLT1-AKT1 axis as the key effector underlying VEGFA-mediated regulation of MuSC survival. All together, our data support that the VEGFA-FLT1-AKT1 pathway promotes MuSC survival during muscle regeneration, and highlights how the minor expression of select transcripts is sufficient for affecting cell behavior.

Introduction

Skeletal muscle and endothelial cells (ECs) and their progenitors from the trunk and limbs are derived from the somites during early developments. Previous works demonstrated the existence of bipotent progenitors which express both Pax3 and FLK1 (Eichmann et al., 1993; Ema et al., 2006; Esner et al., 2006; Kardon et al., 2002; Tozer et al., 2007). These bipotent progenitors migrate into trunk and limb buds from ventrolateral region of the somites to generate MyoD(+) myogenic cells followed by skeletal muscle and PECAM1(+) ECs followed by vasculatures (Hutcheson and Kardon, 2009; Kardon et al., 2002; Lagha et al., 2009; Mayeuf-Louchart et al., 2016, 2014). In addition, FLK1(+) cells give rise to myogenic cells during development and oncologic transformation (Drummond and Hatley, 2018; Mayeuf-Louchart et al., 2014; Motoike et al., 2003). Lastly, multipotent mesoangioblasts, vessel-associated stem cells, have been identified in embryonic dorsal aorta (Minasi et al., 2002). These cells are able to differentiate into several types of mesodermal tissues including skeletal muscle and ECs (Roobrouck et al., 2011). Interestingly, these myogenic cells show the same morphology as muscle satellite cells (MuSCs), stem cell populations for skeletal muscle, and express a number of myogenic and EC markers such as MyoD, M-cadherin, FLK1 and VE-cadherin (De Angelis et al., 1999). However, it is not clear whether adult MuSCs derived from these bipotent progenitors still maintain canonical EC signals. Curiously, blood vessel-associated myoendothelial cell progenitors that express both myogenic and EC markers, and are able to differentiate into myogenic cells following transplantation have been identified in the interstitial spaces of both murine and human adult skeletal muscle (Tamaki et al., 2002; Zheng et al., 2007; Huang et al., 2014). However, the relationship between these myoendothelial cell progenitors and MuSCs remains unclear.

Vascular endothelial growth factor (VEGF), specifically VEGFA modulates many biological aspects including angiogenesis through its two receptors, FLT1 and FLK1. Although FLK1 possesses stronger signaling capability and the major signaling receptor tyrosine kinase (RTK) for VEGFA, FLT1 has considerably higher affinity for VEGF but weaker cytoplasmic signaling capability. In normal tissue, FLT1 acts as a decoy receptor and a sink trap for VEGF thereby preventing excessive normal and pathological angiogenesis. In addition, there are two co-receptors for VEGFA (NRP1 and NRP2) that function with FLK1 to modulate VEGFA signaling. While VEGF signaling has been extensively studied for its role in development, proliferation, and survival of endothelial cells (ECs), its role in non-vascular systems such as neuron and bone has only recently been appreciated (Liu et al., 2012; Okabe et al., 2014; Poesen et al., 2008). Skeletal muscle tissue is the most abundant producer of VEGFA in the body. It has already been extensively studied in the skeletal muscle fibers in models of *Vegfa* knockout mice (Olfert et al., 2009; Tang et al., 2004; Wagner et al., 2006) as well as *Vegfa* overexpression (Arsic et al., 2004; Bouchentouf et al., 2008; Messina et al., 2007; Yan et al., 2005).

Adult skeletal muscle also contains the tissue resident muscle stem cell population, termed MuSCs, which mediate postnatal muscle growth and muscle regeneration (Motohashi and Asakura, 2014). After muscle injury, quiescent MuSCs initiate proliferation to produce myogenic precursor cells, or myoblasts. The myoblasts undergo multiple rounds of cell division before terminal differentiation and formation of multinucleated myotubes by cell fusion. Importantly, the MuSC-derived myoblasts also express VEGFA, which has been shown to increase the proliferation of myoblasts (Christov et al., 2007). Our data obtained from genetical model mice demonstrated that MuSCs express abundant VEGFA, which recruits ECs to establish vascular niche for MuSC self-renewal and maintenance (Verma et al., 2018). In addition, VEGFA and its

receptors are expressed in the myoblast cell line, C2C12 cells, and the signaling can induce cell migration and protect apoptotic cell during myogenic differentiation *in vitro* (Bryan et al., 2008; Germani et al., 2003; Mercatelli et al., 2010). However, it is not clear whether MuSCs also express VEGF receptors and if cell-autonomous VEGFA signaling plays an essential roles in MuSC fucction during muscle regeneration *in vivo*.

We have previously shown that *Flt1* heterozygous gene knockout and conditional deletion of *Flt1* in ECs display increased capillary density in skeletal muscle, indicating the essential roles for *Flt1* in adult skeletal muscle. More importantly, when crossed with the Duchenne muscular dystrophy (DMD) model *mdx* mice, these mice show both histological and functional improvements of their dystrophic phenotypes. This was due to the effect of increased ECs leading to an increase in MuSCs (Verma et al., 2010; Verma et al., 2019). However, the effect of VEGFA on MuSC *in vivo* remained unknown. We found that MuSCs express low levels of canonical EC markers including VEGF receptors using single cell transcriptomics. Therefore, we examined the effects of VEGFA on MuSCs and show that it has a drastic effect on cell survival in the via its receptor FLT1 by signaling through AKT1.

Results

EC gene signal including *Vegf receptors* in MuSCs

EC signatures in MuSCs has been seen in several gene expression data sets (Figure S1A-D, Table S1) (Fukada et al., 2007; Ryall et al., 2015; van Velthoven et al., 2017; Yue et al., 2020). However, with the lack of EC control, we questioned whether these were true expression or artifact. To isolate EC and MuSC populations, we first crossed the $Flk1^{+/GFP}$ mice to label the ECs of the vasculature (Ema et al., 2006) and the $Pax7^{+/CreERT2}$:$ROSO26^{+/Loxp\text{-}stop\text{-}Loxp\text{-}tdTomato}$

105 (*Pax7*$^{+/CreERT2}$:*R26R*$^{+/tdT}$) mice to mark the MuSC lineage (Murphy et al., 2011; Verma et al.,
106 2018). We performed bulk RNA sequencing (RNAseq) on FACS sorted ECs and MuSCs as well
107 as freshly isolated single muscle fibers (Figure 1A, S1E-G). We found that single muscle fibers
108 routinely have ECs fragments attached to the fiber (Figure S1G) and so we removed such fibers
109 based of Flk1^{GFP} expression from the samples collected for sequencing. We surveyed for
110 canonical genes for each cell type (Figure 1B) and found minimal but reliable expression of
111 canonical ECs genes such as *Pecam1*, *Cdh5*, *Kdr*, and *Flt1* in MuSCs.

112 It is possible that these EC signatures detecting in MuSCs were not due to small amounts
113 of contaminating ECs with very high expression of the canonical EC genes skewing the average
114 expression in MuSC RNA samples. To rule out this possibility, we performed single cell
115 RNAseq (scRNAseq) on MuSCs and ECs isolated from mouse hind limb muscle from both basal
116 condition and 3-days post injury to look at both quiescent and activated MuSCs from the reporter
117 mice specified above (Figure 1A). We could reliably delineate injured and activated MuSCs via
118 side and forward scatter (Figure S1H, S1I). We FACS isolated cells from both days separately
119 and spiked in 20% of the ECs into the MuSCs, and performed scRNAseq for each time point
120 (Figure 1A). We performed sequencing with ~300K read/cell compared with the commonly used
121 sequencing with 60K reads/cell, in order to maximize the possibility of detecting low abundance
122 transcripts (Zhang et al., 2020). In the aggregated dataset, the MuSCs showed low overlap
123 between D0 and D3 owing to the different stages of the myogenic differentiation cycle, while the
124 ECs clusters showed near perfect overlap (Figure 1C, 1D). While drastic morphological changes
125 in ECs have been shown during muscle regeneration (Hardy et al., 2016), transcriptomic changes
126 are much more tapered, especially compared with MuSCs (Latroche et al., 2017). We were able
127 to deconvolve the quiescent MuSCs from the activated and differentiating MuSCs, ECs, and

other cell types from gene signatures. (Figure S1J). We also introduced an artificial chromosome loci in our sequencing reference genome to allow for mapping of custom genes such as *eGFP-SV40* and *tdTomato-WPRE-BGHPolyA* transgenes and were able to confirm high expression of these genes to their respective clusters (Figure 1E). Importantly, data from scRNAseq were able to recapitulate the minimal expression of canonical EC genes in the MuSC clusters such as *Cdh5* (Figure 1E) as seen in our Bulk RNAseq results (Figure 1B). These included the *Vegf receptors Flk1* (*Kdr*) and *Flt1* (Figure 1E). As a quality control measure, we mapped parts of the three transgene genes, *eGFP* from $Flk1^{+/GFP}$, and *tdTomato* and *CreERT2* from $Pax7^{+/CreERT2}$:$R26R^{+/tdT}$ that can be detected in ECs and MuSCs, respectively, as expected (Figure S1K).

Surprisingly, we also found *eGFP* in the MuSCs and *tdTomato* in EC fraction, while the *CreERT2* expression remained mainly restricted to the MuSCs (Figure S1K). FACS analysis and FACS-sorted cells confirmed that GFP(+) and tdTomato(+) cells are exclusively restricted as ECs and MuSCs, respectively (Figure S1E, S1F). Therefore, we hypothesized that this was due to the ambient free mRNA from the digested cells that is intrinsic to any droplet based single cell sequencing platform. By using SoupX (Young and Behjati, 2018), we performed careful background subtraction using genes expressed exclusively in myofibers as our negative control and genes validated by *in situ* hybridization as a positive control (Figure S1K) (Kann and Krauss, 2019). We observed decreased but sustained *eGFP* expression in the MuSC fraction and *tdTomato* expression in the EC fraction after SoupX subtraction (Figure S1K). In addition, the EC signatures such as *Cdh5* expression in the MuSC fraction was also sustained. These results conclude that MuSCs contain mRNAs from canonical ECs genes. We showed that the canonical EC genes were broadly expressed in the myogenic cells in our dataset (Figure 1E).

Since detection of rare subpopulation in single cell dataset is a factor of cell numbers, we re-analyzed previously published dataset with 2,232 myogenic cells across different states (Torre et al., 2018; De Micheli et al., 2020). We were able to classify cell as quiescent, proliferative vs. differentiating states based on the expression of *Calcr*, *Cdk1* and *Myog*, respectively (Figure S1L). We noticed that EC prototypic markers such as *Flt1* are broadly expressed with small amounts in MuSCs. Complementary data from different laboratories showed the clear expression of EC prototypic markers such as *Cdh5*, *Flt1* and *Kdr*, using microarrays and Bulk-RNAseq (Figure S1A, S1B; Fukada et al., 2007; Ryall et al., 2015). Recently, RNAseq data from fixed quiescent, early activated and late activated MuSCs show that *Flt1* may be transiently upregulated during the early activation process (Figure S1C) (Yue et al., 2020). To confirm whether the EC gene mRNAs were transcribed from MuSCs, we utilized previously published MuSC nascent RNA transcriptome from TU-tagged samples (Gay et al., 2013; van Velthoven et al., 2017). As expected, *Myh1* was represented in the whole muscle but was absent in the TU-tagged MuSCs (Figure 1F), indicating that the nascent MuSCs were devoid of cellular contamination from other cells in the muscle. Inversely, the nascent MuSC transcript was over-represented for MuSC related genes such as *Calcr* and *Sdc4*. Interestingly, we were able to detect EC genes such as *Kdr* and *Pecam1* in the TU-tagged MuSC samples indicating that they were actively transcribed by MuSCs (Figures 1F, S1D).

We also verified the expression of *Vegfr* genes (*Kdr*, *Flt1*, *Nrp1* and *Nrp2*) in MuSCs using RT-qPCR (Figure 1G). In addition, we verified the expression of *Flt1* by performing *in-situ* hybridization using RNAScope on MuSC on whole muscle fiber, which we currently believe to be the gold standard for expression studies (Figure 1H). Finally, in MuSC-derived myoblasts, NRP1and NRP2 expression was detectable with comparable intensity compared with EC cell

line, while FLT1 expression was detectable with lower intensity compared with EC cell line (Figure 1I). By contrast, PECAM1, VE-Cadherin and FLK1 expression, which was clearly detected in EC cell line, was undetectable level in myoblasts. Taken together, these data indicate that there are both transcripts of these EC canonical genes and EC canonical proteins in MuSCs.

VEGFA induces proliferation and cell survival but not differentiation in myoblasts

Since VEGFRs were expressed in MuSCs in small amounts and their ligand, VEGFA, was highly expressed in MuSCs (Figure 2A; Verma et al., 2018), we wanted to investigate whether there were any biological effects to induction by VEGFA. We found that treatment with VEGFA could increase proliferation of MuSC-derived myoblasts at low dose but inhibit proliferation at high dose of VEGFA, a phenomenon that has been previously described in ECs (Noren et al., 2016)) (Figure S2A). We saw no effect on differentiation by VEGFA as evaluated by myosin heavy chain (MyHC) staining, fusion index and RT-qPCR (Figure S2B, S2C, S2D). By contrast, crystal violet staining showed that VEGFA could significantly increase survived cell number of myoblasts following UV-mediated apoptotic cell death induction (Figure S2E, S2F). To investigate apoptosis in detail, we optimized Annexin V assay following thapsigargin-mediated endoplasmic reticulum (ER)-stress (Hirai et al., 2010) so that we could study deviation at ~ED50 while still performing experiments to remove the confounding variable to proliferation from the experimental setup (Figure S2G and S2H). We had previously shown that MuSCs are the predominant cells that secrete VEGFA in skeletal muscle (Figure 2A; Verma et al., 2018) and while adding exogenous VEGFA did not improve cell survival, blocking VEGFA via a soluble form of FLT1-FC increased the number of apoptotic and necrotic myoblasts *in vitro* (Figure 2C-E).

196

197 **VEGFA-facilitated cell survival in MuSC-derived myoblasts is mediated through FLT1**

198 To characterize the VEGF receptor responsible for the anti-apoptotic effect of VEGFA on
199 MuSC-derived myoblasts, we used pharmacological inhibitors of the VEGF receptors (Figure
200 2F). We used blocking antibody for the VEGF receptors FLT1 (anti-FLT1 antibody), small
201 molecule inhibitors for FLK1 (SU4502 and ZM306416) and the FLK1 co-receptor NRP1
202 (EG00229) (Figure 2D). Surprisingly, inhibiting FLK1, the major signaling RTK for VEGFA,
203 had no effect on myoblasts survival (Figure 3E). By contrast, blocking FLT1 via blocking
204 antibody greatly decreased the survival of myoblasts following thapsigargin induction (Figure
205 3E). To confirm this interesting result using genetic tools, we obtained myoblasts with *Pax7-*
206 *CreER*-inducible deletion of *Flt1* mice ($Pax7^{+/CreER}$:$Flt1^{Loxp/Loxp}$ or *MuSC-*$Flt1^{\Delta/\Delta}$) and the control
207 mice ($Pax7^{+/+}$:$Flt1^{Loxp/Loxp}$). *In vitro* 4-OHT-mediated genetic deletion of *Flt1* (MuSC-$Flt1^{\Delta/\Delta}$)
208 resulted in down-regulation of *Flt1* RNA and FLT1 protein expression (Figure S2I, S2J), and
209 increased spontaneous cell death even without induction of apoptosis (Figure 2F). By contrast,
210 *Flt1* deletion did not affect cell proliferation assessed by EdU staining or myogenic
211 differentiation assessed by MyHC staining (Figure S2K-M). When apoptosis was induced, the
212 *MuSC-*$Flt1^{\Delta/\Delta}$ myoblasts had increased apoptosis that was not responsive to exogenous VEGFA
213 (Figure 2G).

214

215 **AKT signaling is involved in apoptosis of muscle stem cells.**

216 VEGFA signaling is mediated through Extracellular signal-Regulated Kinase (ERK), p38
217 Mitogen-Activated Protein Kinase (MAPK), and Protein kinase B (AKT). In ECs, VEGFA is
218 known to protect cells from apoptosis via AKT (Domigan et al., 2015; Lee et al., 2007).

However, it is not known whether VEGFA can similarly activate AKT in MuSC-derived myoblasts. While the role of AKT has been explored in proliferation and differentiation in myoblasts, its role in apoptosis has not been well characterized (Loiben et al., 2017). We assessed for AKT activation via phosphorylated AKT (pAKT) in MuSC-derived myoblasts. We found that exogenous VEGFA could induce AKT phosphorylation (pAKT) (Figure 2H, 2I). This response was blunted in *MuSC-Flt1*$^{\Delta/\Delta}$ myoblasts and was no longer responsive to VEGFA (Figure 2H, 2I). Lastly, we wanted to confirm that AKT activation could improve myoblast survival. We infected lentiviral *E4ORF1* or *MyrAKT* vectors in myoblasts (Figure 2J), both of which gene products have been shown to specifically activate AKT without activating ERK or p38 (Kobayashi et al., 2010). We found that overexpression of either of these genes improved cell survival compared with the control *in vitro* following induction of apoptosis via thapsagargin (Figure 2J). These data establish FLT1-AKT as the cascade linking VEGFA to apoptosis in MuSC-derived myoblasts during muscle regeneration (Figure 2K).

VEGFA-FLT1 pathway protects MuSCs from apoptosis *in vivo*

Endogenous and exogenous VEGFA have been shown to regulate cell survival and protect ECs from apoptosis *in vitro* (Gerber et al., 1998; Lee et al., 2007). To assess whether additional VEGFA had an effect of MuSC behaviors *in vivo*, we used mice carrying the *VEGFA*$^{+/Hyper}$ allele for injury-mediated tibialis anterior (TA) muscle regeneration following $BaCl_2$ injection (Figure 3A, 3B) (Miquerol et al., 1999). MuSC-derived myoblasts from *Pax7*$^{+/tdT}$*:VEGFA*$^{+/Hyper}$ mice showed around 2.8 fold increased expression of *Vegfa* but not the *Vegfrs* compared with myoblasts from wild-type mice (Figure S3A). Interestingly, while treatment with VEGFA alone had no effect on apoptosis *in vitro*, the MuSCs from *Pax7*$^{+/tdT}$*:VEGFA*$^{+/Hyper}$ mice showed

242 decreased cell death in regenerating muscle by 1 day following $BaCl_2$ injection (Figure 3C).
243 Consequently, single muscle fibers from *Pax7*$^{+/tdT}$*:VEGFA*$^{+/Hyper}$ mice showed increased number
244 of MuSCs, compared with those from *Pax7*$^{+/tdT}$*:VEGFA*$^{+/+}$ mice by 28 days following $BaCl_2$
245 injection (Figure 3D). In addition, muscle regeneration was promoted in *VEGFA*$^{+/Hyper}$ mice in
246 the early and late muscle repair processes as judged by fiber diameter (Figures 3B, 3E, 3F, S3B-
247 D).

248 We then performed the reciprocal experiment to investigate the consequence of *Vegfa*
249 loss in MuSCs *in vivo*, and utilized MuSC-specific *Vegfa* knockout mice
250 (*Pax7*$^{+/CreER}$*:VEGFA*$^{Loxp/Loxp}$). We have previously shown that vasculature in the MuSC-
251 *VEGFA*$^{\Delta/\Delta}$ mouse muscle is perturbed and the proximity between the MuSC and EC is increased
252 (Verma et al., 2018). However, the functional consequences of this remained unknown. We
253 confirmed that clear downregulatin of VEGFA protein in MuSC-derived myoblasts isolated from
254 MuSC-*VEGFA*$^{\Delta/\Delta}$ mice (Figure S3E). We noticed that deletion of *Vegfa* in MuSCs in the *MuSC-*
255 *VEGFA*$^{\Delta/\Delta}$ mouse muscle led to an increase in the proportion of dead MuSCs following $BaCl_2$
256 injection (Figure 3G). Consequently, the number of MuSCs in the MuSC-*VEGFA*$^{\Delta/\Delta}$ muscle were
257 significantly reduced following recovery after injury (Figure 3H). There was no difference in the
258 MuSC numbers in MuSC-*VEGFA*$^{\Delta/\Delta}$ muscle at homeostasis. In addition, the muscle had a
259 regenerative defect as indicated by the shift in fiber size distribution and increased adipose
260 following muscle injury (Figure 3B, 3I, 3J, S3F-H). While a limitation of this experiment is that
261 the MuSC fusion into the fiber also deletes *Vegfa* from the fiber themselves, muscle fiber
262 specific deletion of *Vegfa* has not shown to have an effect on fiber size (Delavar et al., 2014).
263 These data indicate that cell intrinsic VEGFA improves cell survival of MuSCs and that loss of
264 MuSC-derived VEGFA results in reduced muscle regeneration.

Since FLT1 but not FLK1 was detected in MuSCs and MuSC-derived myoblasts, we asked whether the *Flt1* had an effect on MuSC survival *in vivo,* we evaluated cell death in MuSCs from *MuSC-Flt1*$^{\Delta/\Delta}$ mouse muscle. We induced muscle regeneration using $BaCl_2$ for 1 day and assessed for cell death in MuSCs. As seen *in vitro*, we found that loss of *Flt1* in MuSCs (Figure S2I, S2J) resulted in increased cell death during early regeneration (Figure 3K). Consequently, single muscle fibers from *MuSC-Flt1*$^{\Delta/\Delta}$ mice showed decreased number of MuSCs, compared with those from *MuSC-Flt1*$^{+/+}$ mice by 28 days following $BaCl_2$ injection (Figure 3L). We also examined the long-term *in vivo* consequence of deleting *Flt1* from MuSC. There was no significant muscle phenotype in MuSC-*Flt1*$^{\Delta/\Delta}$ muscle at homeostasis (Figures 3B, 3M, 3N). However, following injury, the MuSC-*Flt1*$^{\Delta/\Delta}$ muscle had a modest regenerative defect as indicated by the shift in fiber size distribution following muscle injury (Figures 3B, 3M, 3N, S3J-N).

VEGFA-FLT1 pathway regulates muscle pathology in DMD model mice

While angiogenic defects have been reported in the *mdx* mice as well as in golden retrieval muscular dystrophy (GRMD; canine model of DMD) (Latroche et al., 2015; Verma et al., 2019, 2010; Kodippili et al., 2021; Podkalicka et al., 2021), it is not clear whether VEGF family and its receptors are implicated in human dystrophinopathies. We probed the VEGF ligands and receptors in microarrays (Table S1) from skeletal muscles and MuSCs from *mdx* mice (Pallafacchina et al., 2010; Tseng et al., 2002) and skeletal muscles from the *GRMD* (Vieira et al., 2015). *Vegfa* was downregulated in both models (Figure S4A). *Flt1* was also downregulated in *GRMD* but not *mdx* muscles. To examine whether VEGF signaling is altered in DMD patients, we performed gene expression analysis on previously available data from microarrays from

patients with DMD (Chen et al., 2000). We also aggregated and probed microarray data from muscle biopsies of patients with various neuromuscular diseases or of healthy individuals after exercise (Bakay et al., 2006). In the microarray data, *Vegfa* expression was increased after an acute bout of exercise, and *Vegfa* expression was reduced in ALS muscle, BMD muscle, as well as both early and late phases of DMD muscle (Figure S4A). These data indicate that *Vegfa* expression is decreased in dystrophinopathy, and thus may benefit people with DMD by increasing VEGFA as a therapeutic target.

Therefore, we crossed the *MuSC-Flt1*$^{\Delta/\Delta}$ mice with the chronically regenerating DMD model mice (*mdx*) to generate *mdx:MuSC-Flt1*$^{\Delta/\Delta}$ mice, and analyzed long term effects of *Flt1* deletion (Figure 4A, S4B). Importantly, we found a significant decrease in fiber diameter and increased fibrosis (Figures 4B-D, S4C) in TA muscle accompanied by a physiological decease in muscle perfusion as shown by laser Doppler flow at 12 months age (Figure 4E) as well as a functional decline in muscle strength as judged by grip strength both acutely and chronically (Figure 4F).

By contrast, when we crossed the *VEGFA*$^{+/Hyper}$ mice with *mdx* mice (Figure 4A, S4D), we noticed a significant increase in fiber diameter and decreased fibrosis (Figures 4G-I, S4E) in both TA and diaphragm muscle of *mdx:VEGFA*$^{+/Hyper}$ mice accompanied by a physiological increase in muscle perfusion as shown by laser Doppler flow at 12 months age (Figure 4J) as well as a functional increase in muscle strength as judged by grip strength (Figure 4K). These data indicate that VEGFA-FLT1 axis is a therapeutic target for the pathology seen in the *mdx* mice

Discussion

In this report, we performed bulk and single cell RNA sequencing on MuSCs and ECs. Since deep reads can significantly reduce the effect of the technical noise in scRNAseq, it can improve estimation of minor transcriptional state of a given cell (Zhang, 2020). Unexpectedly, we found that MuSCs broadly express EC prototypic markers in small amounts and used multiple different bioinformatics techniques to validate the results. While similar phenomenon in myogenic cells during development and existence of blood vessel-associated myoendothelial cells in the adult skeletal muscle have been previously described, no functional follow up as been performed leading to the questions whether these minor expression profiles were artifacts or functional (De Angelis et al., 1999; Minasi, 2002; Tamaki et al., 2002; Zheng et al., 2007; Roobrouck, 2011; Huang et al., 2014; Charville et al., 2015; Goel et al., 2017; Giordani et al., 2018). Our goal was to see whether this small expression pattern had biological consequences. We ultimately decided to use *Flt1* for further investigations and used RNAscope and immunostaining to validate its expression in MuSCs. We found that *Flt1* indeed exerts a biological function even at a low expression. Signaling through VEGFA-FLT1-AKT can improve cell survival in MuSCs both *in vivo* and *in vitro.*

On a grander scale, our finding of EC prototype markers expressed in MuSC calls into two questions 1) the genes that we used to specify cellular identities and 2) the cellular identity of MuSCs and ECs. The former is important as when we experimentally label, induce or perform Cre-mediated gene knockout experiments based on our assumptions of different gene expression results which may be confounded for these low expressing genes. For example, we have previously investigated both *Flt1* and *Kdr* in mouse muscle using three different reporters and

found them to be negative in MuSCs, thereby disregarding their cell-autonomous effect when evaluating global knockouts (Verma et al., 2018, 2010). It is also possible that EC mRNAs are results of transcription from the cell or a result of mRNA transfer from neighboring cells (Desrochers et al., 2016). Of note, the transmission of *tdTomato* mRNA and protein from *Pax7*$^{+/CreERT2}$*:R26R*$^{+/tdT}$ mice used in this study has been recently shown via exosome, opening up the possibility of transmission of other mRNA from MuSC to ECs (Murach et al., 2020). The later is an interesting phenomenon form a developmental point of view. MuSCs and ECs arise from a bipotent progenitor originated from somites during early development (Kardon et al., 2002; Hutcheson, 2009; Lagha, 2009; Mayeuf-Louchart, 2014; Mayeuf-Louchart, 2016). Therefore, it is possible that there is a permissive chromatin state that allows for expression of reciprocal genes in the two populations. Along the lines of these observations, FLK1(+) or VE-cadherin(+) cells can contribute to myogenic cells *in vitro* and after cell transplantation (Tamaki et al., 2002; Le Grand et al., 2004; Zheng et al., 2007; Huang et al., 2014;), and during development (Drummond and Hatley, 2018; Mayeuf-Louchart et al., 2014; Motoike et al., 2003). Important notion is that the PDGFRα(-)FLK1(+) population exhibited restricted potential to differentiate into the MuSCs in injured muscle (Sakurai et al., 2008). Interestingly, in the zebrafish, exogenous expression of *Etv2* in the fast muscle can lead to transdifferentiation of muscle fibers into functional vessels so there is evidence of cell fate flexibility (Veldman et al., 2013). The potential of EC transdifferentiation was also examined by ETV2 overexpression in five human cell types, skeletal muscle cells, adipose-derived mesenchymal stem cells, umbilical cord-derived mesenchymal stem cells, embryonic lung fibroblast cells and skin fibroblast cells. Among them, human skeletal muscle cells showed the highest amenability for this EC induction following infection with ETV2 lentivirus vector (Yan et al., 2019). Conversely, *Etv2*-deficient

vascular progenitors can differentiate into skeletal muscle cells (Chestnut et al., 2020). It would be interesting to see whether other EC gene signatures also have functional consequences in the MuSC or muscle at large.

We decided to focus on function of *Flt1* among several EC genes expressed in MuSCs for further investigations on MuSC biology. Our pharmacological and genetic analyses demonstrate that MuSC-derived VEGFA has a drastic effect on cell survival in the via its receptor FLT1 by signaling through AKT1. While VEGFA binds to both FLT1 and FLK1, VEGFB and PGF only bind to FLT1. This creates a scenario where PGF and VEGFB binding can sequester FLT1, increasing free VEGFA availability for VEGFA-FLK1 binding which is the major VEGF signaling pathway for many cell types (Vempati et al., 2014). While PGF is not normally expressed in adult tissues, VEGFB is expressed in the MuSCs and muscle fiber (data not shown). Importantly, the VEGFB-FLT1 axis has also been shown to inhibit apoptosis in retina and brain cells in mouse models of ocular neurodegeneration and stroke (Li et al., 2008). While our results cannot rule out the involvement of VEGFB in protection of MuSC apoptosis, we provide evidence from both pharmacological and genetic data to indicate that VEGFA is involved.

Despite drastic effect of VEGFA-FLT1 on apoptosis *in vitro*, the long-term consequences of *in vivo* deletion of *Flt1* in the MuSC compartment were modest compared with deletion of *Vegfa* in the MuSCs unless crossing with *mdx* mice. Although *Vegfa* is required for both MuSC survival and recruitment of vascular niche (Verma et al., 2018), in the steady state, the MuSC turnover may be low enough that the apoptotic stress burden is low. VEGFA improves cell survival during the proliferative stage following injury, however this transient improvement in

377 survival has only a modest impact on the final regenerative process as shown in
378 *mdx:VEGFA*$^{+/Hyper}$ mice.

379 VEGFA and FLT1 targeted therapies are being explored as both pro- and anti-angiogenic
380 therapies for several indications including retinal degeneration, cancer, pre-eclampsia and
381 neuromuscular diseases (Bae et al., 2005; Keifer et al., 2014; Mac Gabhann et al., 2011; Verma
382 et al., 2010; Verma et al., 2019; Bosco et al., 2021; Xin et al., 2021). As these therapies mature,
383 it will be important to ascertain the MuSC-specific effects of VEGFA and FLT1.

384

Materials and Methods

Mice

Flt1$^{LoxP/LoxP}$ were obtained from Gua-Hua Fong (Ho et al., 2012). *B6.Cg-Pax7*$^{tm1(cre/ERT2)Gaka/J}$ (*Pax7*$^{+/CreERT2}$; JAX stock# 017763; Murphy et al., 2011), *B6.Cg-Gt(ROSA)*$^{26Sortm9(CAG-tdTomato)Hze/J}$ (*Ai9*; JAX stock # 007909; Madisen et al., 2010), *VEGFA*$^{+/Hyper}$ (*Vegfatm1.1Nagy/J*; JAX stock# 027314; Miquerol et al., 1999) and *B6Ros.Cg-Dmd*$^{mdx-5cv}$*/J* (*mdx*^{5cv}; JAX stock #002379; Chapman et al., 1989) were obtained from Jackson Laboratory. *Kdr*$^{tm2.1Jrt/J}$ (*Flk1*$^{+/GFP}$) were obtained from Masatsugu Ema (Ema et al., 2006). *B6.Cg-Pax7*$^{tm1(cre/ERT2)Gaka/J}$ (*Pax7*$^{+/CreERT2}$) mice were crossed with the *B6.Cg-Gt(ROSA)*$^{26Sortm9(CAG-tdTomato)Hze/J}$ (*Ai9*) to yield the *Pax7*$^{+/CreERT2}$*:R26R*^{tdT}(*Pax7*^{tdT}) mice. *Pax7*^{tdT} mice were bred with the *VEGFA*$^{+/Hyper}$ and *Flk1*$^{+/GFP}$ to obtain *Pax7*$^{+/tdT}$*:VEGFA*$^{+/Hyper}$ and *Pax7*$^{+/tdT}$*:Flk1*$^{+/GFP}$ mice. *VEGFA*$^{LoxP/LoxP}$ mice obtained from Napoleone Ferrara (Gerber et al., 1999) were crossed with *Pax7*$^{+/CreERT2}$ to yield the *Pax7*$^{+/CreERT}$*: VEGFA*$^{LoxP/LoxP}$ mice. *Flt1*$^{LoxP/LoxP}$ mice obtained from Guo-Hua Fong (Ho et al., 2012) were crossed with *Pax7*$^{+/CreERT2}$ to yield the *Pax7*$^{+/CreERT}$*:Flt1*$^{LoxP/LoxP}$ mice. Colonies for all the mice were established in the laboratory. Cre recombination was induced using tamoxifen (Sigma-Aldrich, T5648) dosed as 75 mg/kg body weight x 3 times over one week at 3-6 weeks of age. Mice carrying the wild-type *CreERT2* allele were used for control experiments. TA muscle regeneration was induced by intramuscular injection of 20 µl of 1% $BaCl_2$ (Sigma-Aldrich, 342920) or 20 µl of 10 µM Cardiotoxin (CTX) (Sigma-Aldrich, V9125). Mice used for this study is summeried in Table S2.

Genotyping to detect the transgenic and mutant alleles was performed by PCR using the primers described on the web site of Jackson Laboratory shown in Table S3. All primers were synthesized as custom DNA oligos from Integrated DNA technologies (IDT). Genotyping to

detect the mutated allele of *mdx*^{5cv} was performed by PCR using the primers (0981 and 0982) shown in Table S1. The PCR product DNA was digested with *Dra*III restriction enzyme (New England Biolabs, R3510S). Wild-type allele generated 180 bp and mutant allele generated 50 and 130 bp bands.

The animals were housed in an SPF environment and were monitored by the Research Animal Resources (RAR) of the University of Minnesota. All protocols were approved by the Institutional Animal Care and Usage Committee (IACUC) of the University of Minnesota and complied with the NIH guidelines for the use of animals in research.

Cell isolation by FACS

Pax7^{tdT}*:Flk1*^{GFP} mice were utilized for FACS-mediated MuSC and EC isolation as previously described (Asakura et al, 2002; Verma, 2018). We performed extensive validation of the fluorescent reporter mice as previously described (Figure S1A-C; Verma, 2018). Briefly, quiescnet MuSCs and ECs were isolated from the hind limb skeletal muscle of 1–2-mo-old *Pax7*^{tdT}*:Flk1*^{GFP} mice after digestion with collagenase type II. FACS was performed on an FACS sorter (BD FACSAria) and data were analyzed using FlowJo (BD Biosciences). Sorting gates, tdTomato(+) for MuSCs and GFP(+) for ECs, were strictly defined based on control cells isolated from wild-type mice and the forward scatter and side scatter gating. Sorted cells were immediately characterized by immunostaining on slide glasses, utilzed for RNA preparation or cultured on collagen-coated plates in the myoblast growth medium as below to obtain MuSC-derived myoblasts and ECs. FACS analysis was performed as previously described (Turaç et al., 2013). Cells were either trypsinized (cultured cells) or a single cell suspension was obtained following enzymatic digestion as whole muscle-derived cells (Asakura, 2002). Cells were then

washed with FACS buffer (2% BSA and 1 mM EDTA in PBS) followed by live/dead staining using ZombieNIR (Biolegends, 423105). Cells were washed, then immunostained for cell surface markers. Blocking cells was performed with 1% BSA/PBS, and cells were incubated in fluorescently-conjugated antibody. FACS was performed on a Fortessa X-20 (BD Biosciences) with a 355 nm, 405 nm, 488 nm, 561 nm, and 640 nm lasers.

Cell culture

MuSC-derived myoblast isolation from adult mice was performed as previously described (Asakura et al, 2001; Motohashi et al., 2014). Briefly, after collagenase type II (Worthington, CLS-2) treatment, dissociated cells from mouse hindlimb muscle were incubated with anti-CD31-PE (eBiosciences, 12-0311), anti-CD45-PE (eBiosciences, 30-F11), anti-Sca1-PE (eBiosciences, Dec-81) and anti-Integrin α7 (MBL International, ABIN487462), followed by anti-PE microbeads (Miltenyi Biotec, 130-048-801), and then performed LD column (Miltenyi Biotec, 130-042-901) separation. Negative cell populations will be incubated with anti-Mouse IgG beads (Miltenyi Biotec, 130-048-402), and then MS coulumn (Miltenyi Biotec, 130-042-201) separation was performed to isolate Integrin α7(+) MuSCs. MuSC-derived myoblasts were maintained in culture on collagen coated plates in myoblast medium containing 20% FBS and 20 ng/ml bFGF (Invitrogen, PHG0263) in HAM's-F10 medium. Cell cultures were maintained in a humidified incubator at 37°C with 5% CO_2 and 5% O_2. 4-hydroxy tamoxifen (4-OHT, Sigma-Aldrich, H6278) treatment (1 μM in EtOH) was used to induce *Flt1* deletion in myoblasts isolated from $Flt1^{LoxP/LoxP}$:$Pax7^{CreERT2}$ mice. For cell survival assay, 1 x 10^5 cells were allowed to adhere for one day and starved overnight in 0.1% FBS in HAM's F10 medium. Then, cells were exposed to 1 μM EdU along with or withpout 2-100 ng/ml recombinant VEGFA (R&D Systems,

493-MV) for 8 hours before being fixed and stained by the Click-iT EdU Alexa Fluor 488 Imaging Kit (Thermo Scientific, C10337). For induction of apoptosis in myoblasts, (1-2 x 10^5) cells were allowed to adhere to the plates for 16 hours. Thapsigargin-mediated apoptosis was induced by 1 μM of thapsigargin (Sigma-Aldrich, T9033) dissolved in EtOH with or without VEGFA, 100 ng/ml recombinant FLT1-FC (R&D Systems, 7756-FL), 1 μg/ml anti-FLT1 monoclonal antibody (Angio-Proteomie, MAB7072), inhibitors of FLK1, 3 μM ZM306416 (R&D Systems, 2499/1) and 10 μM of SU5402 (R&D Systems, 3300/1) and an inhibitor of NRP1, 30 μM of EG00229 (R&D Systems, 6986/10) for 24 hours. UV light-mediated apoptosis was induced by exposing the cells to UV light in cell culture hood for 45 seconds without medium. After UV exposure, cell survival was assessed 24 hours following culture in 0.1% FBS in HAM's F10 medium with or without VEGFA using the Crystal violet Assay Kit (Abcam, ab232855) and quantated the Crystal violet dye after solubilization by absorbance at 570 nm. To induce differentiation of myoblasts, the myoblast medium was replaced with differentiation medium that contained DMEM supplemented with 5% horse serum with or withour VEGFA or bFGF for 1 or 3 days followed by anti-sarcomeric myosin heavy chain antibody (Developmental Study Hybridoma Bank, MF-20).

AKT induction

The lentiviral pCCL-E4ORF1 and pCCL-myrAkt1 constructs were a kind gift from Dr. Jason Butler (Kobayashi et al., 2010). 293FT cells (Thermo Fisher Scientific, R70007) were seeded in DMEM with 10% FBS and transfected with the lentivirus vectors along with pCMV-VSV-G (Addgene, 8454), pRSV-Rev (Addgene, 12253), and pMDLg/pRRE (Addgene, 12251) using PolyJet transfection reagent (Signagen Laboratories, SL100688). The culture supernatant of the

transfected 293FT cells was added to MuSC-derived myoblast culture with 0.8 μg/ml polybrene (MilliporeSigma, H9268). pAKT1(+) cells were stainined with anti-pAKT antibody (Cell Signaling, 4060).

Apoptosis assay

Apoptosis was measured using measured using Annexin V-Biotin Apoptosis Detection Kit (eBioscience™, BMS500BT-100) as per the manufacture's instruction. Streptavidin-conjugated AlexaFluro-488 was used for detection. Propidium Iodide (PI) was used in all assays except when Pax7tdT(+) cells were utilized or when ZombieNIR (Biolegends, 423105) was used. FACS was performed on a Fortessa X-20 (BD Biosciences) equipped with a 355 nm, 405 nm, 488 nm, 561 nm, and 640 nm lasers.

Immunostaining of cells

Immunostaining for PECAM1, VE-Cadherin, VEGFA, VEGFRs was performed on collagen coated coverslips. Other immunostaining was performed on 30 mm tissue culture plates. Cells were fixed with 2% PFA for 5 minutes and immunostained as previously described (Verma et al., 2010). For membrane receptor staining, cells were permeabilized with 0.01% saponin (ThermoFisher Scientific, ICN10285525) which was kept in the staining solution until the primary antibodies were washed off. At which time, 0.01% Triton-X was added to all the buffers. The antibodies used for this study are listed in Table S4.

Single muscle fiber isolation and staining

Extensor digitorum longus (EDL) muscle was dissected and digested with 0.2% collagenase type I (Sigma-Aldrich, C0130) for single muscle fiber isolation as previously described (Verma et al., 2010). Single muscle fibers were fixed with 2% PFA/PBS, permeabilized with 0.2% Triton-X100 and counterstained with DAPI. Anti-Pax7 antibody(+) or tdTomato(+) MuSCs per single muscle fiber were counted manually.

RNAscope

RNAscope for *Flt1* transcripts was performed as previously described (Kann and Krauss, 2019) on single muscle fibers from *Pax7*^{tdT} mice using the RNAscope Probe - Mm-Flt1 (C1) (ACDBio, 415541). Briefly, isolated EDL fibers are fixed in 4% PFA, washed with PBS, and dehydrated in 100% methanol. Subsequently, fibers are rehydrated in a stepwise gradient of decreasing methanol concentrations in PBS/0.1% Tween-20. Fibers are treated with a proteinase for 10 minutes, followed by hybridization, amplification, and fluorophore conjugation steps.

Histology

The mouse tibialis anterior (TA) muscle was used for all histological analysis. Tissues were frozen fresh using LiN_2 chilled isopentane and stored at -80ºC. Eight µm thick transverse cryosections were used for all histological analysis. Hematoxylin & Eosin (HE) staining were performed as previously described (Verma et al., 2010). Sirius red (Direct Red 80, Sigma-Aldrich, 365548) staining was performed for muscle sections for fibrosis as previously described (Shimizu-Motohashi et al., 2015). Muscle sections were stained in Oil Red O solution (Sigma-Aldrich, O1391-250ML) as previously described (Wang et al., 2017). Microscopic images were captured by a DP-1 digital camera attached to BX51 fluorescence microscope with 10x or 40×

UPlanFLN objectives with cellSens Entry 1.11 (all from Olympus). Photoshop (Adobe) and Fiji (NIH) were used for image processing and manually enumerating the fiber diameter (Schindelin et al., 2012).

Grip strength test

Forelimb grip strength test was performed following a previously published procedure (Aartsma-Rus and van Putten, 2014). Briefly, mice were gently pulled by the tail after fore limb-grasping a metal bar attached to a force transducer (Grip Strength Meter, Columbus Instruments, 1027CSM-D52). Grip strength tests were performed by the same blinded examiner. Five consecutive grip strength tests were recorded, and then mice were returned to the cage for a resting period of 20 minutes. Then, three series of pulls were performed each followed by 20 min resting period. The average of the three highest values out of the 15 values collected was normalized to the body weight for comparison.

Muscle perfusion

RBC flux was evaluated using the moorLabTM laser Doppler flow meter as previously described (Verma, 2010) with the MP7a probe that allows for collecting light from a deeper tissue level than standard probes according to the manufacturer's instructions (Moor Instruments). The fur from the right hind leg was removed using a chemical depilatory. Readings were taken using the probe from at least 10 different spots on the TA muscle. The AU was determined as the average AU value during a plateau phase of each measurement.

RNA and genomic DNA isolation and qPCR

Cultured cells were washed with ice cold PBS and lysed on the place with Trizol™. RNA was isolated using the DirectZol™ RNA Microprep Kit (Zymo Research, R2062) with on-column DNase digestion followed by cDNA synthesis using the Transcriptor First Strand cDNA synthesis kit (Roche Molecular Diagnostics, 04379012001) using random primers. Genomic DNA for genotyping was isolated from mouse tail snips with lysis buffer containing Proteinase K (Sigma-Aldrich, P2308). qPCR was performed using GoTaq qPCR Master Mix (Promega, A6002). The input RNA amount was normalized across all samples and *18S rRNA* or *HtatsF1* was used for normalization of qPCR across samples. Primer sequences are listed in Table S3. All primers were synthesized as custom DNA oligos from Integrated DNA technologies (IDT).

Single cell RNAsequencing and analysis

Cells for single cell RNAseq were obtained from hind limb muscles of 2-3 moth-old *Pax7^{tdT}:Flk1^{GFP}* mice following enzymatic digestion as previously described (Liu et al., 2015). Dead cells were excluded from the analysis using ZombieNIR (Biolegends, 423105). TdTomato(+) and GFP(+) cells were sorted individually and then 20% of GFP(+) cells were spiked into 80% tdTomato(+). We loaded ~5,000 cells into 1 channel of the Chromium system for each of these samples and prepared libraries according to the manufacturer's protocol using version 2.0 chemistry (10x Genomics). Following capture and lysis, we synthesized cDNA and amplified for 12 cycles as per the manufacturer's protocol (10x Genomics). The amplified cDNA was used to construct Illumina sequencing libraries that were each sequenced with ~300K read/cell on one lane of an Illumina HiSeq 2500 machine. We used Cell Ranger 3.1 (10X Genomics) to process raw sequencing data. For A custom genome was constructed to include *eGFP-SV40*, *tdTomato-WPRE-BGHPolyA* and *Pax7-IRES-CreERT2* transgenes. Detailed step-

by-step instructions can be found at https://github.com/verma014/10XCustomRef. We carried out analyses of the filtered data using Seurat suite version 3.0 (Stuart et al., 2019) in R studio (RStudio Team, 2020). For cell imputation, we utilized ALRA through the Seurat wrapper with default settings(Linderman et al., 2018). Additional scRNAseq datasets were obtained from GEO and analyzed using the same method as listed above. A myogenic score was calculated based on the expression of *Myog*, *Pax7*, *Myod1* and *Myf5*. Step-by-step instructions for the analysis can be found on https://github.com/verma014/10XCustomRef.

Background Subtraction

10x Genomics scRNAseq platform uses many more droplets than cells and so following a run, there are many droplets that do not have cells. These droplets still get sequenced with some of the RNA that is in the solution. This floating RNA can be used to estimate the "background" in each droplet. A better description of this can be found by the developers of 'SoupX' (Young and Behjati, 2020). Since *Cdh5* expression has previously been verified in MuSCs using RNAscope, we were able to use it as a positive control to remove the background or "soup" from our data. If *Cdh5* is absent from MuSC, we know that the background subtraction was too aggressive and that subtracting the Soup is not reliable in our case. In addition, we know certain genes that are considered to be specific for MuSCs, muscle ECs or muscle fibers based on the bulk RNAseq (Verma et al., 2018). The top 5 genes that are specific to these population (and also detected by 10x) were selected and used to show the background in our data set was 14.40% and 13.89% for the D0 and D3 dataset, respectively. The step-by-step instructions can be found on https://github.com/verma014/10XCustomRef.

591 **Bulk RNAseq and Microarray Analysis**

592 FASTQ files were downloaded from SRA using SRA-toolkit. Sequences were trimmed using
593 trimmomatic to remove adapter contamination and low-quality reads. Trimmed sequences were
594 mapped to mouse mm10 using Hisat2 (Pertea et al., 2016). Transcript assembly was performed
595 using StringTie (Pertea et al., 2016). Cell type specificity was determined as previously
596 described (Verma et al., 2018). Microarray analysis was performed using the Affymetrix
597 Transcriptome Analysis Console (TAC). Samples in each experiment were RNA normalized and
598 the expression was acquired using the Affeymetrix Expression analysis console with gene level
599 expression. Heatmaps were generated in Prism 9 (Graphpad, La Jolla, CA). The code for
600 generating each graph is listed in the following table, along with the link to the data in tabular
601 format.

602

603 **Quantification and Statistical Analysis**

604 Statistical analysis was performed using Prism 9 (Graphpad, La Jolla, CA) or RStudio (RStudio
605 Team, 2020). For comparison between two groups, an unpaired T-test was used. For comparison
606 between multiple groups, a one-way ANOVA was used with multiple comparisons to the control.
607 Distributions were compared using a chi-squared test. Graphing of the data was performed using
608 Prism 9. Vector diagrams were modified using Graphic (Autodesk). All values are means ±SEM
609 unless noted otherwise. * indicates $p < 0.05$, ** indicates $p < 0.01$, *** indicates $p < 0.001$.

610

611 **Data and Software Availability**

612 All the data was obtained from NCBI GEO. Microarrays of mouse MuSCs were obtained from
613 GSE3483 (Fukada et al., 2007). scRNAseq of MuSCs and muscle ECs was performed in this

study (GSE129057). scRNAseq of whole muscle was obtained from GSE143437 (De Micheli et al., 2020). Bulk RNAseq of MuSCs, ECs and single muscle fibers was obtained from GSE108739 (Verma et al., 2018) and GSE64379 (Ryall et al., 2015). Bulk RNAseq of TU-tagged RNA of MuSCs was obtianed from GSE97399 (van Velthoven et al., 2017). Bulk RNAseq of fixed and unfixed MuSCs was obtained from GSE113631 (Yue et al., 2020). Exercise, ALS, DMD, BMD, FSHD GSE3307, Early DMD GSE465, *mdx* GSE466, GRMD GSE69040, Satellite cells GSE15155. All arrays were normalized to their respective controls. All arrays and RNAseq data are listed in Supplemental Table 1 (Table S1).

Acknowledgements

We thank Minnesota Supercomputing Institute, University of Minnesota Imaging Center, University of Minnesota FACS Facility, and University of Minnesota Genomics Center for providing data for this paper. We also thank Jake Trask for critical reading of this paper. We thank Drs. Yosuke Mukouyama (National Institute of Health), Napoleone Ferrara (Genentech), Guo-Hua Fong (University of Connecticut) and Masatsugu Ema (Siga University of Medical Science) for providing $VEGFA^{LoxP/LoxP}$, $Flt1^{LoxP/LoxP}$ and *Flk1-GFP* mice, respectively. This work was supported by NIHT32-GM008244 and NIHF30AR066454 to MV and NIHR01AR062142, NIHR21AR070319, MDA Research Grant, and Regenerative Medicine Minnesota (RMM) Grant to AA.

Competing interests

The authors declare no competing interests.

637 **Reference**

638 Aartsma-Rus A, van Putten M. 2014. Assessing Functional Performance in the Mdx Mouse
639 Model. *J Vis Exp*. doi:10.3791/51303

640 Arsic N, Zacchigna S, Zentilin L, Ramirez-Correa G, Pattarini L, Salvi A, Sinagra G, Giacca M.
641 2004. Vascular endothelial growth factor stimulates skeletal muscle regeneration in vivo.
642 *Mol Ther* **10**:844–854. doi: 10.1016/j.ymthe.2004.08.007

643 Asakura A, Komaki M, Rudnicki M. 2001. Muscle satellite cells are multipotential stem cells
644 that exhibit myogenic, osteogenic, and adipogenic differentiation. *Differentiation* **68**:245–
645 253. doi: 10.1046/j.1432-0436.2001.680412.x.

646 Asakura A, Seale P, Girgis-Gabardo A, Rudnicki MA. 2002. Myogenic specification of side
647 population cells in skeletal muscle. *J Cell Biol* **159**:123–134. doi: 10.1083/jcb.200202092.

648 Bae DG, Kim TD, Li G, Yoon WH, Chae CB. 2005. Anti-flt1 peptide, a vascular endothelial
649 growth factor receptor 1-specific hexapeptide, inhibits tumor growth and metastasis. *Clin*
650 *Cancer Res* **11**:2651–2661. doi: 10.1158/1078-0432.CCR-04-1564

651 Bakay M, Wang Z, Melcon G, Schiltz L, Xuan J, Zhao P, Sartorelli V, Seo J, Pegoraro E,
652 Angelini C, Shneiderman B, Escolar D, Chen Y-W, Winokur ST, Pachman LM, Fan C,
653 Mandler R, Nevo Y, Gordon E, Zhu Y, Dong Y, Wang Y, Hoffman EP. 2006. Nuclear
654 envelope dystrophies show a transcriptional fingerprint suggesting disruption of Rb-MyoD
655 pathways in muscle regeneration. *Brain* **129**:996–1013. doi:10.1093/brain/awl023

656 Bosco J, Zhou Z, Gabriëls S, Verma M, Liu N, Miller BK, Gu S, Lundberg DM, Huang Y,
657 Brown E, Josiah S, Meiyappan M, Traylor MJ, Chen N, Asakura A, De Jonge N, Blanchetot
658 C, de Haard H, Duffy HS, Keefe D. 2021. VEGFR-1/Flt-1 inhibition increases
659 angiogenesis and improves muscle function in a mouse model of Duchenne muscular

dystrophy. Mol Ther Methods Clin Dev. **23**:21:369-381. doi: 10.1016/j.omtm.2021.03.013

Bouchentouf M, Benabdallah BF, Bigey P, Yau TM, Scherman D, Tremblay JP. 2008. Vascular endothelial growth factor reduced hypoxia-induced death of human myoblasts and improved their engraftment in mouse muscles. *Gene Ther* **15**:404–414. doi: 10.1038/sj.gt.3303059

Bryan BA, Walshe TE, Mitchell DC, Havumaki JS, Saint-Geniez M, Maharaj AS, Maldonado AE, D'Amore PA, Bryan BA, Walshe TE, Mitchell DC, Havumaki JS, Saint-Geniez M, Maharaj AS, Maldonado AE, D'Amore PA. 2008. Coordinated vascular endothelial growth factor expression and signaling during skeletal myogenic differentiation. *Mol Biol Cell* **19**:994–1006. doi:10.1091/mbc.E07-09-0856

Charville GW, Cheung TH, Yoo B, Santos PJ, Lee GK, Shrager JB, Rando TA. 2015. Ex Vivo Expansion and In Vivo Self-Renewal of Human Muscle Stem Cells. *Stem cell Reports* **5**:621–32. doi:10.1016/j.stemcr.2015.08.004

Chen YW, Zhao P, Borup R, Hoffman EP. 2000. Expression profiling in the muscular dystrophies: identification of novel aspects of molecular pathophysiology. *J Cell Biol* **151**:1321–36. doi:10.1083/jcb.151.6.1321

Chestnut B, Casie Chetty S, Koenig AL, Sumanas S. 2020. Single-cell transcriptomic analysis identifies the conversion of zebrafish Etv2-deficient vascular progenitors into skeletal muscle. *Nat Commun* **11**:2796. doi:10.1038/s41467-020-16515-y

Christov C, Chretien F, Abou-Khalil R, Bassez G, Vallet G, Authier FJ, Bassaglia Y, Shinin V, Tajbakhsh S, Chazaud B, Gherardi RK. 2007. Muscle satellite cells and endothelial cells: close neighbors and privileged partners. *Mol Biol Cell* **18**:1397–1409. doi: 10.1091/mbc.e06-08-0693

683 De Angelis L, Berghella L, Coletta M, Lattanzi L, Zanchi M, Cusella-De Angelis MG, Ponzetto
684 C, Cossu G. 1999. Skeletal myogenic progenitors originating from embryonic dorsal aorta
685 coexpress endothelial and myogenic markers and contribute to postnatal muscle growth and
686 regeneration. *J Cell Biol* **147**:869–877. doi:10.1083/jcb.147.4.869
687 De Micheli AJ, Laurilliard EJ, Heinke CL, Ravichandran H, Fraczek P, Soueid-Baumgarten S,
688 De Vlaminck I, Elemento O, Cosgrove BD. 2020. Single-Cell Analysis of the Muscle Stem
689 Cell Hierarchy Identifies Heterotypic Communication Signals Involved in Skeletal Muscle
690 Regeneration. *Cell Rep* **30**:3583-3595.e5. doi:10.1016/j.celrep.2020.02.067
691 Delavar H, Nogueira L, Wagner PD, Hogan MC, Metzger D, Breen EC. 2014. Skeletal myofiber
692 VEGF is essential for the exercise training response in adult mice. *AJP Regul Integr Comp*
693 *Physiol* **306**:R586–R595. doi:10.1152/ajpregu.00522.2013
694 Desrochers LM, Antonyak MA, Cerione RA. 2016. Extracellular Vesicles: Satellites of
695 Information Transfer in Cancer and Stem Cell Biology. Dev Cell. 37(4):301-309. doi:
696 10.1016/j.devcel.2016.04.019.
697 Domigan CK, Warren CM, Antanesian V, Happel K, Ziyad S, Lee S, Krall A, Duan L, Torres-
698 Collado AX, Castellani LW, Elashoff D, Christofk HR, van der Bliek AM, Potente M,
699 Iruela-Arispe ML. 2015. Autocrine VEGF maintains endothelial survival through regulation
700 of metabolism and autophagy. *J Cell Sci* **128**:2236–48. doi:10.1242/jcs.163774
701 Drummond CJ, Hatley ME. 2018. A Case of mistaken identity: Rhabdomyosarcoma
702 development from endothelial progenitor cells. *Mol Cell Oncol* **5**:e1448246.
703 doi:10.1080/23723556.2018.1448246
704 Eichmann A, Marcelle C, Bréant C, Le Douarin NM. 1993. Two molecules related to the VEGF
705 receptor are expressed in early endothelial cells during avian embryonic development. *Mech*

Dev **42**:33–48. doi:10.1016/0925-4773(93)90096-g

Ema M, Takahashi S, Rossant J. 2006. Deletion of the selection cassette, but not cis-acting elements, in targeted Flk1-lacZ allele reveals Flk1 expression in multipotent mesodermal progenitors. *Blood* **107**:111–7. doi:10.1182/blood-2005-05-1970

Esner M, Meilhac SM, Relaix F, Nicolas J-F, Cossu G, Buckingham ME. 2006. Smooth muscle of the dorsal aorta shares a common clonal origin with skeletal muscle of the myotome. *Development* **133**:737–49. doi:10.1242/dev.02226

Fukada S, Uezumi A, Ikemoto M, Masuda S, Segawa M, Tanimura N, Yamamoto H, Miyagoe-Suzuki Y, Takeda S. 2007. Molecular signature of quiescent satellite cells in adult skeletal muscle. *Stem Cells* **25**:2448–59. doi:10.1634/stemcells.2007-0019

Gay L, Miller MR, Ventura PB, Devasthali V, Vue Z, Thompson HL, Temple S, Zong H, Cleary MD, Stankunas K, Doe CQ. 2013. Mouse TU tagging: a chemical/genetic intersectional method for purifying cell type-specific nascent RNA. *Genes Dev* **27**:98–115. doi:10.1101/gad.205278.112

Gerber HP, McMurtrey A, Kowalski J, Yan M, Keyt B a, Dixit V, Ferrara N. 1998. Vascular endothelial growth factor regulates endothelial cell survival through the phosphatidylinositol 3'-kinase/Akt signal transduction pathway. Requirement for Flk-1/KDR activation. *J Biol Chem* **273**:30336–43. doi : 10.1074/jbc.273.46.30336

Germani A, Di Carlo A, Mangoni A, Straino S, Giacinti C, Turrini P, Biglioli P, Capogrossi MC. 2003. Vascular endothelial growth factor modulates skeletal myoblast function. *Am J Pathol* **163**:1417–1428. doi: 10.1016/S0002-9440(10)63499-2

Giordani L, He GJ, Negroni E, Sakai H, Law JYC, Siu MM, Wan R, Corneau A, Tajbakhsh S, Cheung TH, Le Grand F. 2018. High-Dimensional Single-Cell Cartography Reveals Novel

729 Skeletal Muscle Resident Cell Populations. *SSRN Electron J* 1–13.
730 doi:10.2139/ssrn.3249467

731 Goel AJ, Rieder MK, Arnold HH, Radice GL, Krauss RS. 2017. Niche Cadherins Control the
732 Quiescence-to-Activation Transition in Muscle Stem Cells. *Cell Rep* **21**:2236–2250.
733 doi:10.1016/j.celrep.2017.10.102

734 Hardy D, Besnard A, Latil M, Jouvion G, Briand D, Thépenier C, Pascal Q, Guguin A, Gayraud-
735 Morel B, Cavaillon J-M, Tajbakhsh S, Rocheteau P, Chrétien F. 2016. Comparative Study
736 of Injury Models for Studying Muscle Regeneration in Mice. *PLoS One* **11**:e0147198.
737 doi:10.1371/journal.pone.0147198

738 Hirai H, Verma M, Watanabe S, Tastad C, Asakura Y, Asakura A. 2010. MyoD regulates
739 apoptosis of myoblasts through microRNA-mediated down-regulation of Pax3. *J Cell Biol*
740 **191**:347–65. doi:10.1083/jcb.201006025

741 Ho VC, Duan L-J, Cronin C, Liang BT, Fong G-H. 2012. Elevated vascular endothelial growth
742 factor receptor-2 abundance contributes to increased angiogenesis in vascular endothelial
743 growth factor receptor-1-deficient mice. *Circulation* **126**:741–52.
744 doi:10.1161/CIRCULATIONAHA.112.091603

745 Huang P, Schulz TJ, Beauvais A, Tseng YH, Gussoni E. 2014.
746 Intramuscular adipogenesis is inhibited by myo-endothelial progenitors with functioning
747 Bmpr1a signalling. Nat Commun. 5:4063. doi: 10.1038/ncomms5063.

748 Hutcheson DA, Kardon G. 2009. Genetic manipulations reveal dynamic cell and gene functions:
749 Cre-ating a new view of myogenesis. *Cell Cycle* **8**:3675–8. doi:10.4161/cc.8.22.9992

750 Kann AP, Krauss RS. 2019. Multiplexed RNAscope and immunofluorescence on whole-mount
751 skeletal myofibers and their associated stem cells. *Dev* **146**. doi:10.1242/dev.179259

752 Kardon G, Campbell JK, Tabin CJ. 2002. Local extrinsic signals determine muscle and
753 endothelial cell fate and patterning in the vertebrate limb. *Dev Cell* **3**:533–45.
754 doi:10.1016/s1534-5807(02)00291-5
755 Keifer OP, O'Connor DM, Boulis NM. 2014. Gene and protein therapies utilizing VEGF for
756 ALS. *Pharmacol Ther* **141**:261–71. doi:10.1016/j.pharmthera.2013.10.009
757 Kobayashi H, Butler JM, O'Donnell R, Kobayashi M, Ding B-S, Bonner B, Chiu VK, Nolan DJ,
758 Shido K, Benjamin L, Rafii S. 2010. Angiocrine factors from Akt-activated endothelial cells
759 balance self-renewal and differentiation of haematopoietic stem cells. *Nat Cell Biol*
760 **12**:1046–56. doi:10.1038/ncb2108
761 Kodippili K, Thorne PK, Laughlin MH, Duan D. 2021. Dystrophin deficiency impairs vascular
762 structure and function in the canine model of Duchenne muscular dystrophy. *J Pathol*.
763 doi:10.1002/path.5704
764 Lagha M, Brunelli S, Messina G, Cumano A, Kume T, Relaix F, Buckingham ME. 2009.
765 Pax3:Foxc2 reciprocal repression in the somite modulates muscular versus vascular cell fate
766 choice in multipotent progenitors. *Dev Cell* **17**:892–9. doi:10.1016/j.devcel.2009.10.021
767 Latroche C, Matot B, Martins-Bach A, Briand D, Chazaud B, Wary C, Carlier PG, Chrétien F,
768 Jouvion G. 2015. Structural and Functional Alterations of Skeletal Muscle Microvasculature
769 in Dystrophin-Deficient mdx Mice. *Am J Pathol* 1–13. doi:10.1016/j.ajpath.2015.05.009
770 Latroche C, Weiss-Gayet M, Muller L, Gitiaux C, Leblanc P, Liot S, Ben-Larbi S, Abou-Khalil
771 R, Verger N, Bardot P, Magnan M, Chrétien F, Mounier R, Germain S, Chazaud B. 2017.
772 Coupling between Myogenesis and Angiogenesis during Skeletal Muscle Regeneration Is
773 Stimulated by Restorative Macrophages. *Stem Cell Reports* **9**.
774 doi:10.1016/j.stemcr.2017.10.027

775 Le Grand F, Auda-Boucher G, Levitsky D, Rouaud T, Fontaine-Pérus J, Gardahaut M-F. 2004.
776 Endothelial cells within embryonic skeletal muscles: a potential source of myogenic
777 progenitors. *Exp Cell Res* **301**:232–41. doi:10.1016/j.yexcr.2004.07.028
778 Lee S, Chen TT, Barber CL, Jordan MC, Murdock J, Desai S, Ferrara N, Nagy A, Roos KP,
779 Iruela-Arispe ML. 2007. Autocrine VEGF signaling is required for vascular homeostasis.
780 *Cell* **130**:691–703. doi:10.1016/j.cell.2007.06.054
781 Li Y, Zhang F, Nagai N, Tang Z, Zhang S, Scotney P, Lennartsson J, Zhu C, Qu Y, Fang C, Hua
782 J, Matsuo O, Fong GH, Ding H, Cao Y, Becker KG, Nash A, Heldin CH, Li X. 2008.
783 VEGF-B inhibits apoptosis via VEGFR-1-mediated suppression of the expression of BH3-
784 only protein genes in mice and rats. *J Clin Invest* **118**:913–923. doi:10.1172/JCI33673
785 Linderman GC, Zhao J, Kluger Y. 2018. Zero-preserving imputation of scRNA-seq data using
786 low-rank approximation. *bioRxiv* 397588. doi**:** https://doi.org/10.1101/397588
787 Liu L, Cheung TH, Charville GW, Rando T a. 2015. Isolation of skeletal muscle stem cells by
788 fluorescence-activated cell sorting. *Nat Protoc* **10**:1612–1624. doi:10.1038/nprot.2015.110
789 Liu Y, Berendsen AD, Jia S, Lotinun S, Baron R, Ferrara N, Olsen BR. 2012. Intracellular
790 VEGF regulates the balance between osteoblast and adipocyte differentiation. *J Clin Invest*
791 **122**:3101–3113. doi:10.1172/JCI61209
792 Loiben AM, Soueid-Baumgarten S, Kopyto RF, Bhattacharya D, Kim JC, Cosgrove BD. 2017.
793 Data-Modeling Identifies Conflicting Signaling Axes Governing Myoblast Proliferation and
794 Differentiation Responses to Diverse Ligand Stimuli. *Cell Mol Bioeng* **10**:433–450.
795 doi:10.1007/s12195-017-0508-5
796 Mac Gabhann F, Qutub AA, Annex BH, Popel AS. 2011. Systems biology of pro-angiogenic
797 therapies targeting the VEGF system. *Wiley Interdiscip Rev Syst Biol Med* **2**:694–707.

798 doi:10.1002/wsbm.92

799 Mayeuf-Louchart A, Lagha M, Danckaert A, Rocancourt D, Relaix F, Vincent SD, Buckingham
800 M. 2014. Notch regulation of myogenic versus endothelial fates of cells that migrate from
801 the somite to the limb. *Proc Natl Acad Sci U S A* **111**:8844–8849.
802 doi:10.1073/pnas.1407606111

803 Mayeuf-Louchart A, Montarras D, Bodin C, Kume T, Vincent SD, Buckingham M. 2016.
804 Endothelial cell specification in the somite is compromised in Pax3-positive progenitors of
805 Foxc1/2 conditional mutants, with loss of forelimb myogenesis. *Development* **143**:872–9.
806 doi:10.1242/dev.128017

807 Mercatelli N, Dimauro I, Ciafré SA, Farace MG, Caporossi D. 2010. AlphaB-crystallin is
808 involved in oxidative stress protection determined by VEGF in skeletal myoblasts. *Free*
809 *Radic Biol Med* **49**:374–82. doi:10.1016/j.freeradbiomed.2010.04.027

810 Messina S, Mazzeo A, Bitto A, Aguennouz M, Migliorato A, De Pasquale MG, Minutoli L,
811 Altavilla D, Zentilin L, Giacca M, Squadrito F, Vita G. 2007. VEGF overexpression via
812 adeno-associated virus gene transfer promotes skeletal muscle regeneration and enhances
813 muscle function in mdx mice. *FASEB J* **21**:3737–3746. doi : 10.1096/fj.07-8459com

814 Minasi MG, Riminucci M, De Angelis L, Borello U, Berarducci B, Innocenzi A, Caprioli A,
815 Sirabella D, Baiocchi M, De Maria R, Boratto R, Jaffredo T, Broccoli V, Bianco P, Cossu G.
816 2002. The meso-angioblast: a multipotent, self-renewing cell that originates from the dorsal
817 aorta and differentiates into most mesodermal tissues. *Development* **129**:2773–83. doi:
818 10.1242/dev.129.11.2773

819 Miquerol L, Gertsenstein M, Harpal K, Rossant J, Nagy a. 1999. Multiple developmental roles
820 of VEGF suggested by a LacZ-tagged allele. *Dev Biol* **212**:307–322.

doi:10.1006/dbio.1999.9355

Motohashi N, Asakura A. 2014. Muscle satellite cell heterogeneity and self-renewal. *Front Cell Dev Biol* **2**:1–11. doi:10.3389/fcell.2014.00001

Motohashi N, Asakura Y, Asakura A. 2014. Isolation, culture, and transplantation of muscle satellite cells. *J Vis Exp* 1–7. doi:10.3791/50846

Motoike T, Markham DW, Rossant J, Sato TN. 2003. Evidence for novel fate of Flk1+ progenitor: contribution to muscle lineage. *Genesis* **35**:153–9. doi:10.1002/gene.10175

Murach KA, Vechetti IJ, Van Pelt DW, Crow SE, Dungan CM, Figueiredo VC, Kosmac K, Fu X, Richards CI, Fry CS, McCarthy JJ, Peterson CA. 2020. Fusion-Independent Satellite Cell Communication to Muscle Fibers During Load-Induced Hypertrophy. *Function* **1**:1–15. doi:10.1093/function/zqaa009

Murphy MM, Lawson J a, Mathew SJ, Hutcheson D a, Kardon G. 2011. Satellite cells, connective tissue fibroblasts and their interactions are crucial for muscle regeneration. *J Cell Sci* **124**:e1–e1. doi:10.1242/jcs098228

Noren DP, Chou WH, Lee SH, Qutub AA, Warmflash A, Wagner DS, Popel AS, Levchenko A. 2016. Endothelial cells decode VEGF-mediated Ca2+ signaling patterns to produce distinct functional responses. *Sci Signal* **9**:ra20–ra20. doi:10.1126/scisignal.aad3188

Okabe K, Kobayashi S, Yamada T, Kurihara T, Tai-nagara I. 2014. Neurons Limit Angiogenesis by Titrating VEGF in Retina. *Cell* **159**:584–596. doi:10.1016/j.cell.2014.09.025

Olfert IM, Howlett RA, Tang K, Dalton ND, Gu Y, Peterson KL, Wagner PD, Breen EC. 2009. Muscle-specific VEGF deficiency greatly reduces exercise endurance in mice. *J Physiol* **587**:1755–1767. doi: : 10.1113/jphysiol.2008.164384

Pallafacchina G, François S, Regnault B, Czarny B, Dive V, Cumano A, Montarras D,

844 Buckingham M. 2010. An adult tissue-specific stem cell in its niche: a gene profiling
845 analysis of in vivo quiescent and activated muscle satellite cells. *Stem Cell Res* **4**:77–91.
846 doi:10.1016/j.scr.2009.10.003
847 Pertea M, Kim D, Pertea GM, Leek JT, Salzberg SL. 2016. Transcript-level expression analysis
848 of RNA-seq experiments with HISAT, StringTie and Ballgown. *Nat Protoc* **11**:1650–1667.
849 doi:10.1038/nprot.2016.095
850 Podkalicka P, Mucha O, Kaziród K, Bronisz-Budzyńska I, Ostrowska-Paton S, Tomczyk M,
851 Andrysiak K, Stępniewski J, Dulak J, Łoboda A. 2021. Age-Dependent Dysregulation of
852 Muscle Vasculature and Blood Flow Recovery after Hindlimb Ischemia in the mdx Model
853 of Duchenne Muscular Dystrophy. Biomedicines. 9:481. doi:
854 10.3390/biomedicines9050481.
855 Poesen K, Lambrechts D, Van Damme P, Dhondt J, Bender F, Frank N, Bogaert E, Claes B,
856 Heylen L, Verheyen A, Raes K, Tjwa M, Eriksson U, Shibuya M, Nuydens R, Van Den
857 Bosch L, Meert T, D'Hooge R, Sendtner M, Robberecht W, Carmeliet P. 2008. Novel Role
858 for Vascular Endothelial Growth Factor (VEGF) Receptor-1 and Its Ligand VEGF-B in
859 Motor Neuron Degeneration. *J Neurosci* **28**:10451–10459. doi:10.1523/JNEUROSCI.1092-
860 08.2008
861 Roobrouck VD, Clavel C, Jacobs SA, Ulloa-Montoya F, Crippa S, Sohni A, Roberts SJ, Luyten
862 FP, Van Gool SW, Sampaolesi M, Delforge M, Luttun A, Verfaillie CM. 2011.
863 Differentiation potential of human postnatal mesenchymal stem cells, mesoangioblasts, and
864 multipotent adult progenitor cells reflected in their transcriptome and partially influenced by
865 the culture conditions. *Stem Cells* **29**:871–82. doi:10.1002/stem.633
866 RStudio Team. 2020. RStudio: Integrated Development for R. RStudio, PBC, Boston, MA.

http://www.rstudio.com/

Ryall JG, Dell'Orso S, Derfoul A, Juan A, Zare H, Feng X, Clermont D, Koulnis M, Gutierrez-Cruz G, Fulco M, Sartorelli V. 2015. The NAD+-dependent sirt1 deacetylase translates a metabolic switch into regulatory epigenetics in skeletal muscle stem cells. *Cell Stem Cell* **16**:171–183. doi:10.1016/j.stem.2014.12.004

Sakurai H, Okawa Y, Inami Y, Nishio N, Isobe K. 2008. Paraxial mesodermal progenitors derived from mouse embryonic stem cells contribute to muscle regeneration via differentiation into muscle satellite cells. *Stem Cells* **26**:1865–73. doi:10.1634/stemcells.2008-0173

Schindelin J, Arganda-Carreras I, Frise E, Kaynig V, Longair M, Pietzsch T, Preibisch S, Rueden C, Saalfeld S, Schmid B, Tinevez J-Y, White DJ, Hartenstein V, Eliceiri K, Tomancak P, Cardona A. 2012. Fiji: an open-source platform for biological-image analysis. *Nat Methods* **9**:676–82. doi:10.1038/nmeth.2019

Stuart T, Butler A, Hoffman P, Hafemeister C, Papalexi E, Mauck WM, Hao Y, Stoeckius M, Smibert P, Satija R. 2019. Comprehensive Integration of Single-Cell Data. *Cell* **177**:1888-1902.e21. doi:10.1016/j.cell.2019.05.031

Tamaki T, Akatsuka A, Ando K, Nakamura Y, Matsuzawa H, Hotta T, Roy RR, Edgerton VR. 2002. Identification of myogenic-endothelial progenitor cells in the interstitial spaces of skeletal muscle. *J Cell Biol* **157**:571–7. doi:10.1083/jcb.200112106

Tang K, Breen EC, Gerber H-P, Ferrara NM a, Wagner PD. 2004. Capillary regression in vascular endothelial growth factor-deficient skeletal muscle. *Physiol Genomics* **18**:63–69. doi:10.1152/physiolgenomics.00023.2004

Torre E, Dueck H, Shaffer S, Gospocic J, Gupte R, Bonasio R, Kim J, Murray J, Raj A. 2018.

Rare Cell Detection by Single-Cell RNA Sequencing as Guided by Single-Molecule RNA FISH. *Cell Syst* **6**:171-179.e5. doi:10.1016/j.cels.2018.01.014

Tozer S, Bonnin M-A, Relaix F, Di Savino S, García-Villalba P, Coumailleau P, Duprez D. 2007. Involvement of vessels and PDGFB in muscle splitting during chick limb development. *Development* **134**:2579–91. doi:10.1242/dev.02867

Tseng BS, Zhao P, Pattison JS, Gordon SE, Granchelli JA, Madsen RW, Folk LC, Hoffman EP, Booth FW. 2002. Regenerated mdx mouse skeletal muscle shows differential mRNA expression. *J Appl Physiol* **93**:537–45. doi:10.1152/japplphysiol.00202.2002

Turaç G, Hindley CJ, Thomas R, Davis JA, Deleidi M, Karaöz E, Pruszak J. 2013. Combined Flow Cytometric Analysis of Surface and Intracellular Antigens Reveals Surface Molecule Markers of Human Neuropoiesis. *PLoS One* **8**:1–14. doi:10.1371/journal.pone.0068519

van Velthoven CTJ, de Morree A, Egner IM, Brett JO, Rando TA. 2017. Transcriptional Profiling of Quiescent Muscle Stem Cells In Vivo. *Cell Rep* **21**:1994–2004. doi:10.1016/j.celrep.2017.10.037

Veldman MB, Zhao C, Gomez G a, Lindgren AG, Huang H, Yang H, Yao S, Martin BL, Kimelman D, Lin S. 2013. Transdifferentiation of fast skeletal muscle into functional endothelium in vivo by transcription factor etv2. *PLoS Biol* **11**:e1001590. doi:10.1371/journal.pbio.1001590

Vempati P, Popel AS, Mac Gabhann F. 2014. Extracellular regulation of VEGF: Isoforms, proteolysis, and vascular patterning. *Cytokine Growth Factor Rev* **25**:1–19. doi:10.1016/j.cytogfr.2013.11.002

Verma M, Asakura Y, Hirai H, Watanabe S, Tastad C, Fong G-H, Ema M, Call JA, Lowe DA, Asakura A. 2010. Flt-1 haploinsufficiency ameliorates muscular dystrophy phenotype by

913 developmentally increased vasculature in mdx mice. *Hum Mol Genet* **19**:4145–59.
914 doi:10.1093/hmg/ddq334
915 Verma M, Asakura Y, Murakonda BSR, Pengo T, Latroche C, Chazaud B, McLoon LK,
916 Asakura A. 2018. Muscle Satellite Cell Cross-Talk with a Vascular Niche Maintains
917 Quiescence via VEGF and Notch Signaling. *Cell Stem Cell* **23**:530-543.e9.
918 doi:10.1016/j.stem.2018.09.007
919 Verma M, Shimizu-Motohashi Y, Asakura Y, Ennen JP, Bosco J, Zhou Z, Fong G, Josiah S,
920 Keefe D, Asakura A. 2019. Inhibition of FLT1 ameliorates muscular dystrophy phenotype
921 by increased vasculature in a mouse model of Duchenne muscular dystrophy. *PLOS Genet*
922 **15**:e1008468. doi:10.1371/journal.pgen.1008468
923 Vieira NM, Elvers I, Alexander MS, Moreira YB, Eran A, Gomes JP, Marshall JL, Karlsson EK,
924 Verjovski-Almeida S, Lindblad-Toh K, Kunkel LM, Zatz M. 2015. Jagged 1 Rescues the
925 Duchenne Muscular Dystrophy Phenotype. *Cell* **163**:1204–1213.
926 doi:10.1016/j.cell.2015.10.049
927 Wagner PD, Olfert IM, Tang K, Breen EC. 2006. Muscle-targeted deletion of VEGF and
928 exercise capacity in mice. *Respir Physiol Neurobiol* **151**:159–166.
929 doi:10.1016/j.resp.2005.09.007
930 Xin C, Chu X, Wei W, Kuang B, Wang Y, Tang Y, Chen J, You H, Li C, Wang B. 2021.
931 Combined gene therapy via VEGF and mini-dystrophin synergistically improves
932 pathologies in temporalis muscle of dystrophin/utrophin double knockout mice. Hum Mol
933 Genet. 30:1349-1359. doi: 10.1093/hmg/ddab120.
934 Yan G, Yan R, Chen C, Chen C, Zhao Y, Qin W, Veldman MB, Li S, Lin S. 2019. Engineering
935 vascularized skeletal muscle tissue with transcriptional factor ETV2-induced autologous

endothelial cells. *Protein Cell* **10**:217–222. doi:10.1007/s13238-018-0542-7

Yan H, Guo Y, Zhang P, Zu L, Dong X, Chen L, Tian J, Fan X, Wang N, Wu X, Gao W. 2005. Superior neovascularization and muscle regeneration in ischemic skeletal muscles following VEGF gene transfer by rAAV1 pseudotyped vectors. *Biochem Biophys Res Commun* **336**:287–298. doi: 10.1016/j.bbrc.2005.08.066

Young MD, Behjati S. 2020. SoupX removes ambient RNA contamination from droplet based single-cell RNA sequencing data. *bioRxiv* 303727. doi:10.1101/303727

Yue L, Wan R, Luan S, Zeng W, Cheung TH. 2020. Dek Modulates Global Intron Retention during Muscle Stem Cells Quiescence Exit. *Dev Cell* **53**:661-676.e6. doi:10.1016/j.devcel.2020.05.006

Zhang MJ, Ntranos V, Tse D. 2020. Determining sequencing depth in a single-cell RNA-seq experiment. *Nat Commun* **11**:1–11. doi:10.1038/s41467-020-14482-y

Figure Legends

Figure 1. EC gene signal including VEGF receptor genes in MuSCs.

A) Experimental schema for bulk and single cell sequencing from the *Pax7*^{CreERT2}:*R26R*^{tdT}:*Flk1*^{GFP} mice. Bulk sequencing performed on MuSCs, ECs and single muscle fibers (SMFs) from uninjured muscle. FACS sorted MuSCs and ECs from uninjured and regenerating TA muscle (3 days following CTX) were run separately on the 10X single cell platform and aggregated.

B) Bulk RNAseq showing EC signature in MuSCs. Subset dividing genes that are commonly used to delineate cell identity for MuSCs, ECs and SMFs. Last column shows genes that define macrophages (Mφ), which should not be highly expressed in any on our cell types. Red dots indicate MuSCs, green dots indicate ECs and blue dots indicate SMFs.

C) UMAP from aggregated single cell RNAseq shows expression of different phases of MuSCs (quiescent MuSCs, activated MuSCs and myoblasts), ECs (tip ECs and ECs) and from likely contaminant cells such as macrophages (Mφ) and smooth muscle cells (SMC).

D) UMAP from aggregated data visualized by sample day showing MuSCs segregated by the sample day but overlap in the EC population. Red dots indicate intact (day 0) and blue dots indicate 3 days following CTX.

E) Expression of quality control genes such as *eGFP*, *tdTomato*, *CreERT2* and EC genes such as *Cdh5*, *Kdr* and *Flt1*.

F) Genome browser tracks of whole muscle and TU-tagged MuSC nascent RNA (GSE97399, Velthoven et al., 2017). *Kdr* and *Pecam1* expression can be found in the MuSC fraction. As control, *Myh1* is highly expressed in the whole muscle preparation but largely absent in the MuSC fraction. *Sdc4* and *Calcr* are highly expressed in MuSC and less so in the whole muscle fraction.

G) qPCR for *Kdr, Flt1, Nrp1* and *Nrp2* in EC lines (B.end3 and C166), muscle cell line (C2C12) and MuSC-derived myoblasts in growth and differentiation medium (DM) shows low level expression of VEGFRs and VEGF co-receptors.

H) RNAScope of *Flt1* on freshly isolated single muscle fibers from $Pax7^{tdT}$ mice shows *Flt1* expression (green) and tdTomato (red) in MuSCs. Nuclei were counterstained with DAPI (blue). Scale bar indicates 5 µm.

I) Immunostaining for PECAM1, VE-cadherin (VE-Cad), VEGFA co-receptors (NRP1 and NRP2) and VEGFA receptors (FLT1 and FLK1) in B.End3 EC cell line and MuSC-derived myoblasts (MB). Nuclei were counterstained with DAPI (blue). Scale bar indicates 20 µm.

Figure 2. VEGFA-FLT1-AKT1 axis controls apoptosis in MuSC *in vitro.*

A) Immunostaining for VEGFA (green) in MuSC-derived myoblasts. Nuclei were counterstained with DAPI (blue). Scale bar indicates 20 µm.

B) Experimental scheme for assessing apoptosis following thapsagargin induction in myoblast culture.

C) Decreased cell survival in myoblast *in vitro* as VEGFA is blocked using FLT1-FC (a VEFGA trap). This phenotype is partially rescued with exogenous VEGFA (50 ng/ml).

D) Graphical representation of the VEGF pathway inhibitors used in panel D.

E) Following thapsagargin induction, apoptotic and necrotic cells are increased with inhibition of FLT1 via FLT1-FC or anti-FLT1 antibody (anti-FLT1 mAb) but not FLK1 (SU5402 and ZM306416) or NRP1-FLK1 inhibition (EG00229) following exogenous VEGFA (50 ng/ml).

F) 4-OHT induced deletion of *Flt1* in *Pax7*$^{+/CreER}$:*Flt1*$^{Loxp/Loxp}$ myoblasts is sufficient to reduce cell survival in myoblast without induction of apoptosis.

G) Cell survival is decreased *in vitro* in myoblast with thapsagargine induction following 4-OHT mediated deletion of *Flt1* in *Pax7*$^{+/CreER}$:*Flt1*$^{Loxp/Loxp}$ myoblast that is not rescued by exogenous VEGFA. Blue indicates *MuSC-Flt1*$^{+/+}$, red indicates *MuSC-Flt1*$^{+/+}$ with 50 ng/ml VEGFA, green indicates *MuSC-Flt1*$^{\Delta/\Delta}$ and purple indicates *MuSC-Flt1*$^{\Delta/\Delta}$ with 50 ng/ml VEGFA.

H) Representative images of pAKT (red) in myoblast stained by MyoD (green) in *MuSC-Flt1*$^{+/+}$ and *MuSC-Flt1*$^{\Delta/\Delta}$ myoblasts induced with exogenous VEGFA. Nuclei were counterstained with DAPI (blue). Scale bar indicates 50 μm.

I) Quantification of pAKT in myoblasts stained by MyoD in *MuSC-Flt1*$^{+/+}$ and *MuSC-Flt1*$^{\Delta/\Delta}$ myoblast induced w/wo exogenous VEGFA. VEGFA induction increases pAKT in *MuSC-Flt1*$^{+/+}$ myoblasts but this response is lost in *MuSC-Flt1*$^{\Delta/\Delta}$ myoblasts.

J) Annexin V quantification of myoblasts transfected with myr-AKT and E4ORF1 to activate AKT1 showed increased cell survival of myoblasts following apoptosis induction.

K) Representative model for VEGFA-FLT1-AKT axis-mediated MuSC survival.

Figure 3. MuSC-derived *VEGFA* and *Flt1* requires proper skeletal muscle.

A) Experimental schema detailing the experiments performed in this figure. The $Pax7^{+/CreER}$:$R26R^{tdT}$:$VEGFA^{+/Hyper}$ ($VEGFA^{+/Hyper}$) $Pax7^{+/CreER}$:$R26R^{tdT}$:$VEGFA^{Loxp/Loxp}$ *for MuSC-*$VEGFA^{\Delta/\Delta}$ and $Pax7^{tdT}$:$Flt1^{Loxp/Loxp}$ for *MuSC-*$Flt1^{\Delta/\Delta}$ lines were pulsed with tamoxifen (TMX) prior to investigation.

B) Representative H&E-stained images for intact and on 14-day post injury TA muscle from *MuSC-*$VEGFA^{+/Hyper}$, *MuSC-*$Flt1^{\Delta/\Delta}$ *and MuSC-*$VEGFA^{\Delta/\Delta}$ mice and their representative controls. Scale bar indicates 50 µm.

C) Annexin V staining show less necrotic cells in MuSC from $VEGFA^{+/Hyper}$ mice compared with the control one day following injury.

D) Quantification of MuSCs from single muscle fibers show increased MuSCs in $VEGFA^{+/Hyper}$ EDL muscle compared with the control mice at base line and 14 days post injury.

E) Fiber size distribution and F) mean feret's diameter of uninjured and regenerating muscle 14 days post injury from $VEGFA^{+/Hyper}$ and control mice show no difference at baseline but an increase in fiber diameter following injury.

G) Annexin V staining show increased dead cells in MuSCs from *MuSC-*$VEGFA^{\Delta/\Delta}$ mice one day following CTX compared with the control *MuSC-*$VEGFA^{+/+}$ mice.

H) Quantification of MuSCs from single muscle fiber at base line and 14 days post injury.

I) Fiber size distribution and J) mean feret's diameter of uninjured and regenerating muscle 14 days post injury from *MuSC-*$VEGFA^{\Delta/\Delta}$ and *MuSC-*$VEGFA^{+/+}$ mice show no difference at baseline but a decrease in fiber diameter following injury.

K) Annexin V staining show increased apoptosis in MuSCs from *MuSC-Flt1*$^{\Delta/\Delta}$ mice one day following injury compared with the control *MuSC-Flt1*$^{+/+}$ mice.

L) Quantification of MuSCs from single muscle fiber show decreased MuSCs in *MuSC-Flt1*$^{\Delta/\Delta}$ EDL muscle at base line and 14 days post injury compared with the control *MuSC-Flt1*$^{+/+}$ mice.

M) Fiber size distribution and N) mean feret's diameter of uninjured and regenerating muscle from *MuSC-Flt1*$^{\Delta/\Delta}$ and compared with the control *MuSC-Flt1*$^{+/+}$ mice show no difference at baseline but a decrease in fiber diameter following injury.

Figure 4. VEGFA-FLT1 pathway in MuSCs regulates muscle pathology in DMD model mice.

A) Experimental schema detailing the experiments performed in this figure. The *mdx:Pax7*^{tdT}*:Flt1*$^{Loxp/Loxp}$ was pulsed with tamoxifen (TMX) to generate *mdx:MuSC-Flt1*$^{\Delta/\Delta}$ mice prior to investigation. *mdx*:*VEGFA*$^{+/Hyper}$ mouse line was used without any induction.

B) Representative H&E and Sirus red stain from *mdx:MuSC-Flt1*$^{+/+}$ and *mdx:MuSC-Flt1*$^{\Delta/\Delta}$ mouse TA muscle at 3 months of age. Scale bar indicates 50 µm.

C) Smaller average fiber size in *mdx:MuSC-Flt1*$^{\Delta/\Delta}$ compared with the control *mdx:MuSC-Flt1*$^{+/+}$ mouse TA muscle.

D) Increased fibrotic area in *mdx:MuSC-Flt1*$^{\Delta/\Delta}$ compared with the control *mdx:MuSC-Flt1*$^{+/+}$ mouse TA muscle.

E) Decreased muscle perfusion in *mdx:MuSC-Flt1*$^{\Delta/\Delta}$ compared with the control *mdx:MuSC-Flt1*$^{+/+}$ mouse TA muscle.

F) Decreased grip strength normalized to body weight in *mdx:MuSC-Flt1*$^{\Delta/\Delta}$ compared with the control *mdx:MuSC-Flt1*$^{+/+}$ mouse TA muscle at both 3 and 12 months of age.

G) Representative H&E and Sirus red stain from *mdx*:*VEGFA*$^{+/Hyper}$ and *mdx*:*VEGFA*$^{+/+}$ mouse TA muscle at 3 months from TA muscle (top four panels) and diaphragm muscle (bottom four panels).

H) Increased average fiber size in *mdx*:*VEGFA*$^{+/Hyper}$ compared with the control *mdx*:*VEGFA*$^{+/+}$ mouse TA and diaphragm (DM) muscle. Scale bar indicates 50 μm.

I) Decreased fibrosis in *mdx*:*VEGFA*$^{+/Hyper}$ compared with the control *mdx*:*VEGFA*$^{+/+}$ mouse TA and diaphragm (DM) muscle

J) Muscle perfusion is increased in *mdx*:*VEGFA*$^{+/Hyper}$ compared with the control *mdx*:*VEGFA*$^{+/+}$ mouse TA muscle.

K) Grip strength normalized to body weight is increased in *mdx*:*VEGFA*$^{+/Hyper}$ compared with the control *mdx*:*VEGFA*$^{+/+}$ mice.

Figure 1

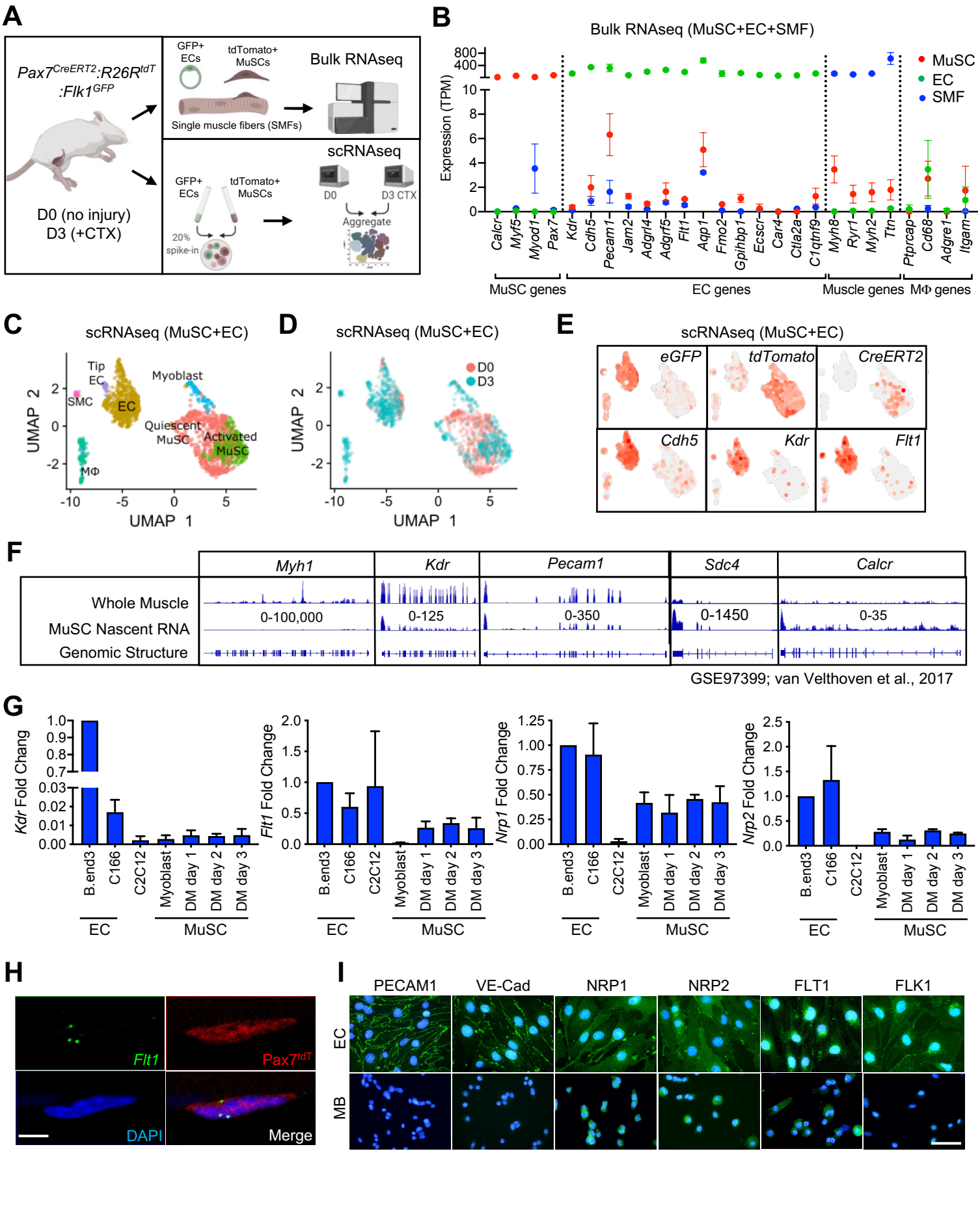

Figure 2

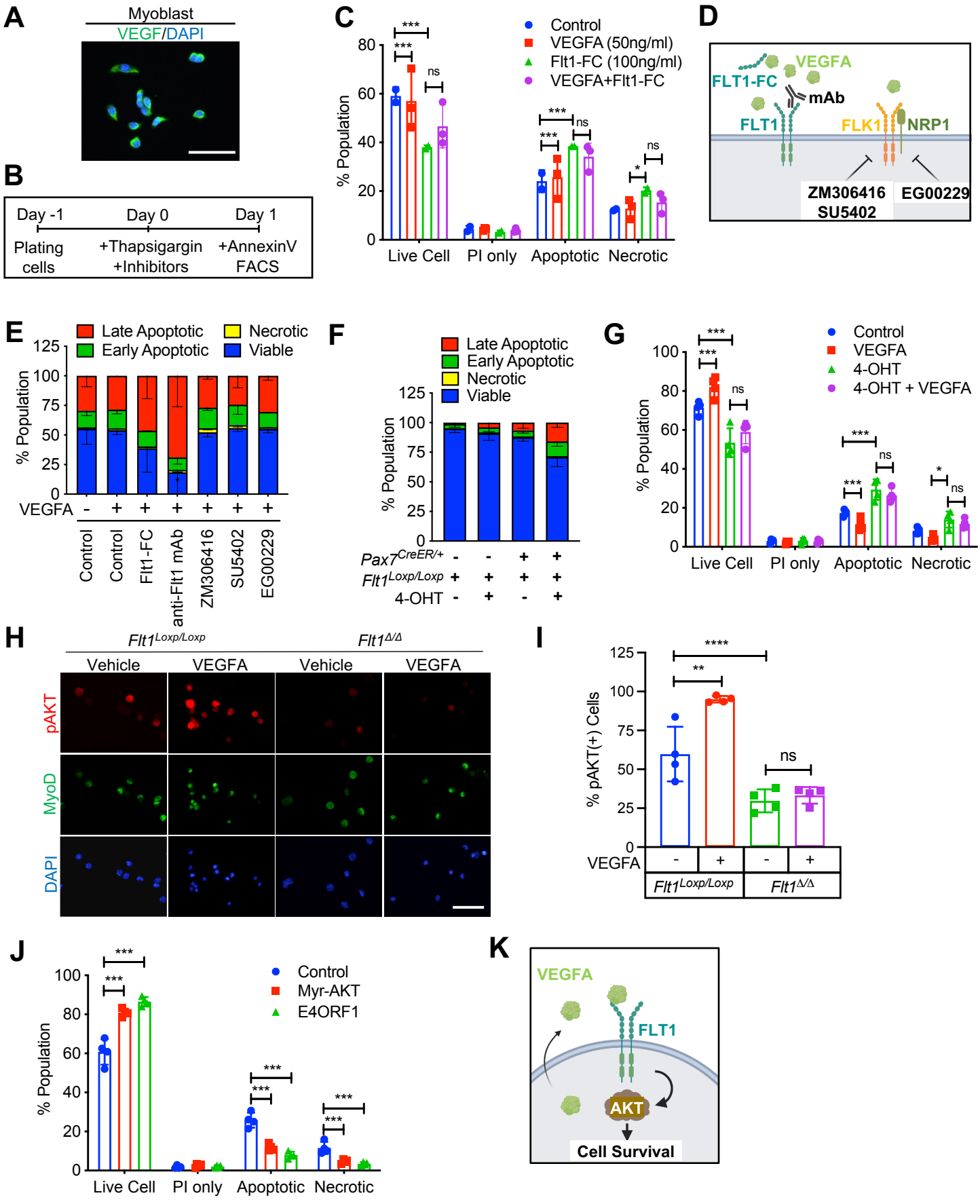

Figure 3

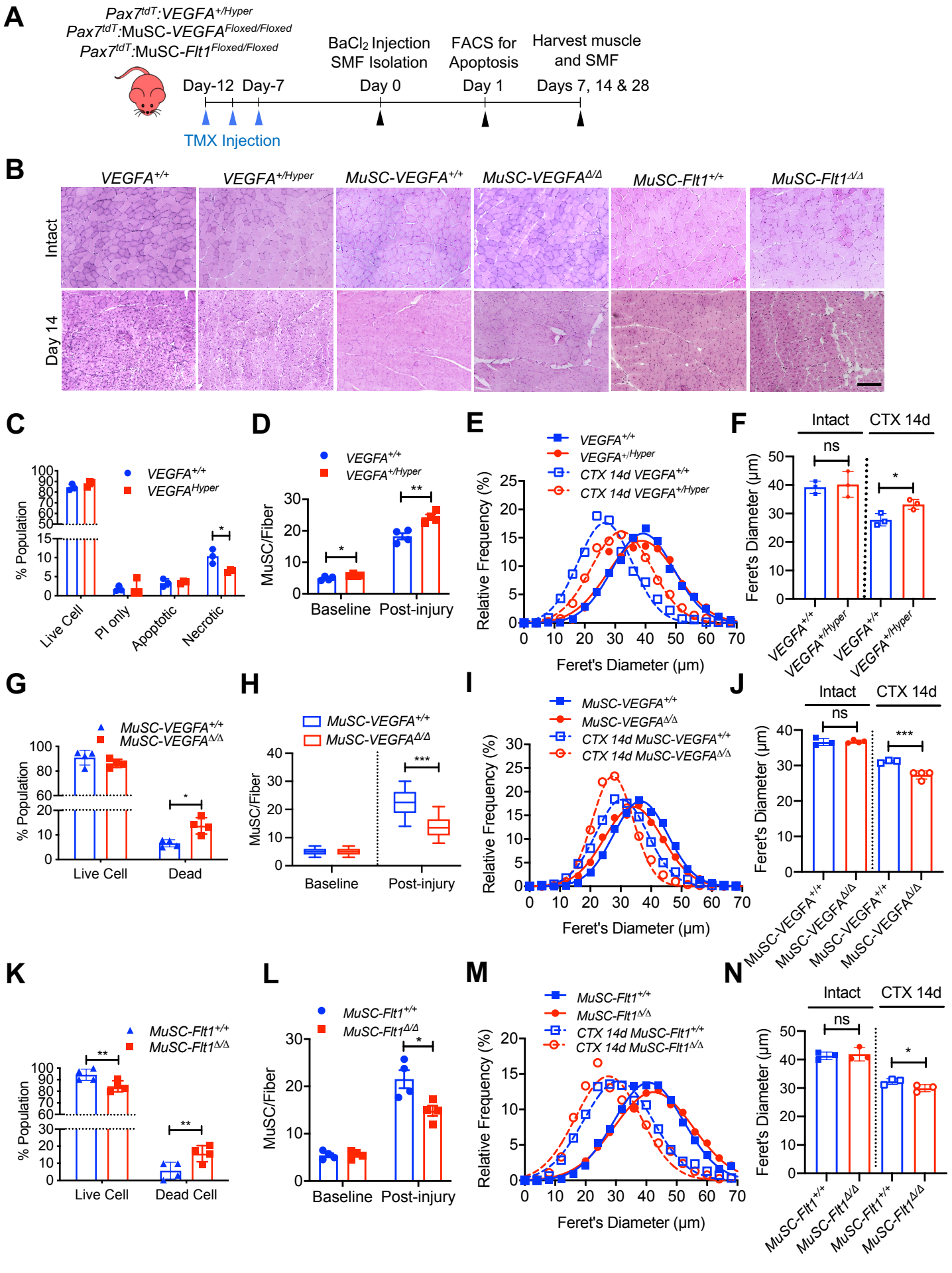

Figure 4